

Abundances on the Main Sequence of Omega Centauri

Laura M. Stanford, G. S. Da Costa and John E. Norris

*Research School of Astronomy and Astrophysics, Australian National University, Weston,
ACT, 2611, Australia*

stanford, gdc, jen@mso.anu.edu.au

and

Russell D. Cannon

Anglo-Australian Observatory, P.O. Box 296, Epping, NSW, 2121, Australia

rdc@aaoepp.gov.au

ABSTRACT

Abundance ratios of carbon, nitrogen and strontium relative to iron, calculated using spectrum synthesis techniques, are given for a sample of main sequence and turnoff stars that belong to the globular cluster ω Centauri. The variations of carbon, nitrogen and/or strontium show several different abundance patterns as a function of $[\text{Fe}/\text{H}]$. The source of the enhancements/depletions in carbon, nitrogen and/or strontium may be enrichment from asymptotic giant branch stars of low ($1\text{--}3 M_{\odot}$) and intermediate ($3\text{--}8 M_{\odot}$) mass. Massive rotating stars which produce excess nitrogen without carbon and oxygen overabundances may also play a role. These abundances enable different contributors to be considered and incorporated into the evolutionary picture of ω Cen.

Subject headings: globular clusters: general — globular clusters: individual (ω Centauri)

1. Introduction

The globular cluster ω Centauri is known to have characteristics not shared by other clusters. Its unusual nature was first noted by Woolley et al. (1966) and Cannon & Stobie (1973), who demonstrated that its red giant branch (RGB) has an intrinsic color spread. Early abundance studies of member stars, obtained spectroscopically, have shown a range

in metallicity (Freeman & Rodgers 1975; Lloyd Evans 1977; Butler, Dickens & Epps 1978; Cohen & Bell 1986; Francois, Spite & Spite 1988; Paltoglou & Norris 1989). In the last decade detailed spectroscopic and photometric work on ω Cen has revealed the large extent of the abundance range within the system.

The cluster metallicity distribution has been studied in more detail recently, using spectroscopic analysis of the Ca II triplet lines (Norris, Freeman & Mighell 1996; Suntzeff & Kraft 1996), photometry (Lee et al. 1999; Pancino et al. 2000; Hilker & Richtler 2000; Sollima et al. 2005a) and spectroscopic analysis of the Ca II K line (Stanford et al. 2006a). These studies found few, if any, stars with $[\text{Fe}/\text{H}] < -2.0$. The distribution then rises to a peak at $[\text{Fe}/\text{H}] = -1.7$ with a long tail to higher metallicities, up to $[\text{Fe}/\text{H}] \approx -0.4$. The distribution also has a second peak at $[\text{Fe}/\text{H}] = -1.2$ (Norris, Freeman & Mighell 1996). Three main populations within the cluster have been identified (Norris, Freeman & Mighell 1996; Suntzeff & Kraft 1996; Pancino et al. 2002). The bulk of the cluster stars ($\sim 70\%$) has metallicities at $[\text{Fe}/\text{H}] \approx -1.7$, the metal-intermediate population has $[\text{Fe}/\text{H}] \approx -1.2$ and represents roughly 20% of the stars, and the remaining 5% of the stars are metal-rich at $[\text{Fe}/\text{H}] \approx -0.6$. Sollima et al. (2005a) found the RGB to be discrete in nature and identified up to five distinct populations, three of which are within the metal-intermediate population described above. Elemental studies have shown a range in abundances within the cluster members. Carbon, nitrogen and oxygen exhibit large scatters for a given $[\text{Fe}/\text{H}]$ (Persson et al. 1980; Brown & Wallerstein 1993; Norris & Da Costa 1995a, hereafter ND95). The α -elements (Mg, Si, Ca and Ti) have constant values at a given $[\text{Fe}/\text{H}]$ for most metallicities (Brown & Wallerstein 1993; Smith et al. 1995; ND95; Smith et al. 2000) but $[\alpha/\text{Fe}]$ decreases at higher metallicities ($[\text{Fe}/\text{H}] > -1.0$) (Pancino et al. 2002). As the α element abundances are constant with iron below $[\text{Fe}/\text{H}] \approx -1.0$, they are produced by the same source, most likely supernovae Type II. At higher abundances, decreasing $[\alpha/\text{Fe}]$ is indicative of supernovae Type Ia contributions.

The heavy neutron-capture elements (e.g. Y, Zr, Ba, La, Pr, Nd) give information on enrichment sources, shedding light on whether a slow or rapid neutron-capture process occurred (or both). ND95 and Smith et al. (1995) found the s-process element abundance ratios with respect to iron increase with increasing $[\text{Fe}/\text{H}]$ and then flatten above $[\text{Fe}/\text{H}] = -1.2$. These results are in contrast to normal globular clusters, and indicate that the stellar winds from asymptotic giant branch (AGB) stars (sources of s-process elements) were involved with the enrichment process of ω Cen. ND95 concluded also that there were no correlations between the abundance ratios with respect to iron for the s-process elements and those for C, N, O, Na and Al. Eu is an r-process element, and abundances of this element are found to be lower in ω Cen stars than in the field (Smith et al. 1995), and ratios of Ba/La show that the enrichment process is dominated by the s-process (ND95).

Another piece in the ω Cen puzzle is the double main sequence seen in deep photometry of the cluster (Anderson et al. 2002; Bedin et al. 2004). This is thought to be the result of helium variations of the order of $\Delta Y \sim 0.12$ dex between two populations (Norris 2004; Piotto et al. 2005). The source of the large amount of additional helium required may be AGB stars with masses larger than $6M_{\odot}$, stellar winds associated with early evolutionary phases of massive stars, or perhaps Type II supernovae (Norris 2004; Piotto et al. 2005; Maeder & Meynet 2006). Bekki & Norris (2006) suggest that the helium enhanced population formed from gas ejected by the stellar populations that surrounded ω Cen when it was the nucleus of a dwarf galaxy. Maeder & Meynet (2006) have argued that in models with low metallicity, massive stars with high rotation can produce the large amounts of helium required to explain the blue main sequence (bMS), depending on the slope of the initial mass function. These models also produce a large excess of nitrogen but little carbon, consistent with the phenomena observed in spectra of the stars in the bMS (Piotto et al. 2005).

Variations of the CNO group, Na, Mg and Al abundances have been found in most *normal* globular clusters on the RGB to different degrees. In the last few decades, studies of main sequence turn off (MSTO) stars in a number of globular clusters have shown that variations exist in C and N in this region of the CMD as well. These clusters include 47 Tuc (Cannon et al 1998; Briley et al 2004), NGC 6752 (Suntzeff & Smith 1991; Gratton et al 2001a), M71 (Cohen 1999; Briley & Cohen 2001; Ramírez & Cohen 2002), M5 (Cohen, Briley & Stetson 2002) and M13 (Briley, Cohen & Stetson 2004). Anticorrelations between Na and O have been shown to exist on the main sequence (MS) in 47 Tuc (Carretta et al. 2004), NGC 6397 and NGC 6752 (Gratton et al 2001b). These latter two clusters also have an anticorrelation between Mg and Al (Gratton et al 2001b).

There are three possibilities for the origin of the abundance variations in ω Cen and other globular clusters: internal processing, accretion of matter onto surface layers, and primordial formation. Firstly, internal processing within the individual stars themselves, with the products then being mixed to the surface layers, may be the source of the abundance variations. This may account, in part, for the variations in the RGB stars in some clusters, as the level of C depletion on the RGB increases with decreasing magnitude (e.g. Langer et al. 1986, M92). However, mixing of the internal layers does not occur in the current MS stars (e.g. Da Costa & Demarque 1982). Therefore, internal processing cannot explain all the variations seen in globular clusters. The second option is that the enriched objects accreted matter onto their surface layers from the stellar winds of AGB stars. The stars may have been a part of a binary system or in the vicinity of AGB stars. The accreted material will be on the surface layers only, and therefore, in a comparison of MS with RGB abundance ratios, one should generally find higher abundances for the unevolved stars compared with the evolved ones as increased convective mixing as the stars evolve up the RGB will dilute

the accreted material. Primordial variations account for the third and final possibility. Here, the stars formed from material that had been previously enriched from sources such as winds and ejecta of AGB stars, massive rotating stars and/or supernovae.

Most spectroscopic studies have concentrated on the red giant branch (RGB) stars in ω Cen because of their greater brightness. We have obtained spectra of a sample of turnoff stars to examine the relationship between age and metallicity in the cluster (Stanford et al. 2006a), and to determine abundances of several elements and compare them with those found on the RGB. This will give further insights into the evolutionary history of ω Cen and enable us to distinguish between surface enhancement and primordial enrichment scenarios within the cluster.

The present paper describes the analysis of these spectra to determine abundances of C, N and strontium, relative to iron, for the MS and turnoff (TO) sample and an attempt to untangle the complex evolutionary history of ω Cen. Early results of this work are given in Da Costa et al. (2005). In § 2 we describe the observations and reduction techniques. § 3 outlines the derivation of metallicities and ages for the sample and discusses the metallicity populations. We describe the techniques used to determine C, N and Sr abundances in § 4. Finally, § 5 summarizes the results and discusses a chemical evolutionary history for the cluster.

2. Observations and Reduction

The observations and reduction of our data are described in detail in Stanford et al. (2006a) to which we refer the reader. Suffice it here to say the photometry of the cluster was obtained with the 1m telescope/Tektronix CCD combination at Siding Spring Observatory in the V and B bands. From these data a CMD, shown in Figure 1, was constructed for objects within an annulus 15–25 arcminutes from the cluster center. Two regions were defined on the upper MS with a view to determining the metallicity and age range for the cluster. Stars in each region were observed using the Two degree Field (2dF) Multiobject spectrograph (Lewis et al. 2002) on the Anglo-Australian Telescope. This spectrograph has the capability of simultaneously observing up to 400 objects using a fibre fed system. The first sample was observed in May 1998 and April 1999 (hereafter 98/99 sample), and the second in March 2002 (hereafter 2002 sample). Figure 1 shows the two boxes from which candidates were selected. Spectra were obtained with 1200 line/mm gratings employed in the spectrographs and covered the wavelength range $\lambda\lambda 3800\text{--}4600\text{\AA}$. They have a resolution of $\sim 2.5\text{\AA}$ FWHM and signal-to-noise (S/N) of 30-50. A final sample of 424 radial velocity selected members was found. The members are shown as large dots in Figure 1. The small dots represent the

photometry of all the remaining objects that do not have membership information.

Data for stars on the MS were also obtained for three other globular clusters — NGC 6397, NGC 6752 and 47 Tuc. These clusters were observed in a similar manner to ω Cen, and membership was determined based on radial velocities and metallicities. The data obtained for the clusters were used to test the reliability of the metallicity calibration, and for comparison of abundances.

3. Metallicities and Populations

The process for calculating metallicities has been described in detail in Stanford et al. (2006a). To summarize, the metallicities were calculated using a combination of two methods (see Beers et al. (1999) for details of these methods briefly described below). The first uses the Ca II K line strength and color of an object to assign a metallicity. Due to the saturation of the Ca II K line these metallicities become uncertain above $[\text{Fe}/\text{H}] \approx -1.0$. The second method utilizes the weak metal lines in the spectrum. This method is reliant on spectra having good signal-to-noise (>30) as the noise can become confused with the weak metal lines. As metal-poor stars have few and very weak metal lines, this method is unreliable at lower metallicities ($[\text{Fe}/\text{H}] < -2.0$) and the abundance from the Ca II K line strength was adopted. Between $[\text{Fe}/\text{H}] = -2.0$ and $[\text{Fe}/\text{H}] = -1.0$ a weighted mean of the two values was used and above $[\text{Fe}/\text{H}] = -1.0$ metallicities from the second method were adopted. Metallicities were calculated for the ω Cen sample, and for the calibrating clusters NGC 6397, NGC 6752 and 47 Tuc. An age was then calculated for each ω Cen star based on its position on the CMD and metallicity using theoretical isochrones (cf. Stanford et al. (2006a)).

The metallicities are used here to divide the samples into three groups, approximate the three main populations in ω Cen. The metal-poor population (1st Pop.) contains stars with $[\text{Fe}/\text{H}] < -1.5$. The metal-intermediate population (2nd Pop.) contains objects that have $-1.5 \leq [\text{Fe}/\text{H}] < -1.1$. The third population (3rd Pop.) contains the stars that have the highest metallicities in our sample with $[\text{Fe}/\text{H}] \geq -1.1$. The histograms of metallicities for our two samples (98/99 and 2002) are shown in Figure 2. The figure also shows the cuts in metallicity that make up the three populations, with 255/424 in the 1st Population, 144/424 in the second and 25/424 in the metal-rich population. The calibrating clusters were used to compare abundances at similar metallicities. The values for these clusters come from Harris (1996). NGC 6397, with $[\text{Fe}/\text{H}] = -1.96$, was compared with the first population. NGC 6752 is borderline between the 1st Pop. and 2nd Pop. with $[\text{Fe}/\text{H}] = -1.56$, and can be used for comparison purposes with both of these populations. 47 Tuc, with $[\text{Fe}/\text{H}] = -0.76$, was used to compare with the 3rd Pop.

The photometry for the three ω Cen populations is plotted in Figure 3. An isochrone (Y², Yi et al. 2001) was fitted to each population on the CMD with parameters depending on the mean metallicity and age for the population. These isochrones are overplotted in Figure 3. Ten points were chosen along the isochrone that encompassed our sample in luminosity and color and the corresponding temperature and gravity were used in the abundance analysis. For the first and second populations (at $[\text{Fe}/\text{H}] = -1.7$ and -1.2 respectively) the $[\alpha/\text{Fe}]$ ratio was taken to be 0.3 (ND95; Smith et al. 1995, 2000). For the most metal-rich population with a mean $[\text{Fe}/\text{H}] = -0.8$, the alpha enhancement was taken to be $[\alpha/\text{Fe}] = 0.18$.

3.1. Indices

Indices were measured for the G band (CH) at $\sim 4300\text{\AA}$, violet CN band at 3883\AA , the Sr II 4077\AA and 4215\AA lines, and Ba II 4554\AA for the ω Cen members and calibrating cluster stars. The weaker Sr II 4215\AA line was used as confirmation of the Sr abundance, which was determined primarily from the SrII 4077\AA feature. The bandpasses for CH, Sr and Ba are given in Table 1 and the indices are defined following Beers et al. (1999). The CN index is S3839 as defined by Norris et al. (1981). The ω Cen data are plotted as a function of metallicity in Figure 4, and are split into main-sequence ($V > 18$) and SGB ($V \leq 18$) samples. The corresponding indices determined for NGC 6397, NGC 6752 and 47 Tuc are represented by boxplots showing the area in $[\text{Fe}/\text{H}]$ -index space they occupy for comparison with the MS ω Cen stars, as we do not have data for the SGB stars in these clusters. The center line within the rectangle for each boxplot represents the median for each dataset. The lower and upper sides of the box represent the first and third quartiles while the vertical lines extending from the upper and lower edges of the box represent the upper and lower limits of the data. The error bars in the figure represent the standard error of the mean of the indices for individual observations, and the derived error in metallicity.

Studying the two CH plots, one can see that the SGB group has, in general, higher indices than on the MS one. This is due to the cooler temperatures on the SGB than the MS. At lower metallicities on the MS, there are two members that have unusually high C indices. These fall well outside the ranges in $[\text{Fe}/\text{H}]$ and the CH index that is occupied by the calibrating clusters. Outliers can also be identified on the SGB. The S3839 index shows several objects which appear to have high abundances of carbon and/or nitrogen in both the MS and SGB groups. The strontium index plot shows a large scatter, with several outliers in each. For the SGB group, a least-squares fit to the data was performed, shown by the solid line. This line indicates there are several objects with considerably higher Sr indices than the main population. There is little spread in the Ba index, most likely due to the low

sensitivity of our data to the Ba abundance.

The CN/CH bimodality known to exist on the RGB of 47 Tuc is also found on the MS (Cannon et al 1998; Da Costa et al. 2004). CN strong and CN weak stars exist in ω Cen on the RGB (Norris & Bessell 1975; Persson et al. 1980; Cohen & Bell 1986; ND95), but have not yet been seen on the MS in ω Cen. Figure 5 plots the CN index versus the CH one for the ω Cen data, and is split into the three metallicity bins as well as the MS and SGB groups (left and right columns respectively). Also plotted, as open circles, are the 47 Tuc data showing the bimodality within this cluster for comparison with the metal-rich, MS population in ω Cen. The solid line is a fit to the 47 Tuc anticorrelation and plotted in each panel as a reference. The dotted line is the one used to define the CN weak/CH strong, and vice versa, groups.

4. First Pass Abundances

To obtain an initial estimate of the abundance ratios of stars in our sample, in particular for the stars that have enhancements in carbon, nitrogen and/or strontium, we compared indices obtained from synthetic spectra with those from the observed data. As described in §3, the ω Cen sample was divided by metallicity into three populations, as shown in Figure 3. Isochrones with the mean metallicity and ages of each population were fitted to the data. Discrete points along these isochrones gave a series of stellar parameters (temperature and gravity) that are representative of the observed data for each population.

Kurucz models (1993) were used with atomic line lists from R. A. Bell (2000, private communication) and Kurucz molecular lines lists to generate synthetic spectra to compare with our observations. The spectrum synthesis code was originally developed by Cottrell & Norris (1978). A synthetic spectrum with appropriate stellar parameters was compared with an atlas of the Sun (Beckers et al. 1976). Using an adopted solar C abundance of $\log(N/N_{tot})=-3.36$, the CH feature showed a small difference between the spectrum of the Sun, and the synthetic spectrum, and as a result the $\log(gf)$ values were reduced by 0.5 dex. Similarly, for an adopted N abundance of $\log(N/N_{tot})=-4.04$, the synthetic violet CN feature was too strong with respect to the solar spectrum and the $\log(gf)$ values were reduced by 0.25 dex. The $\log(gf)$ values for the blue CN feature ($\lambda 4215\text{\AA}$) were reduced by 0.10 dex in a similar manner. The Sr II 4077 and 4215 lines and Ba II 4554 line were also compared and found to be within acceptable agreement. An observed spectrum of Arcturus (α Boo) was then compared with a synthetic spectrum with appropriate stellar parameters (ND95) and was used as an independent check of the adjusted values. It was found to provide acceptable agreement with abundance studies of this star. Table 2 lists the gf values

and solar abundances used here for Sr and Ba.

The derived abundance of C is influenced by the amount of oxygen within the star as the CO molecule forms preferentially over the CH one. However, for our range of stellar parameters, changing the O abundance was demonstrated to have no effect on our calculations. This was tested by generating a series of synthetic spectra at metallicities that spanned the ω Cen metallicity range with several temperatures and gravities typical of the observed sample. The oxygen abundance was varied for each one (between $[O/Fe]=0.0$ and 0.5 dex), and the strength of the G band was compared between synthetic spectra with the same stellar parameters. It was found that oxygen did not play a significant role in the abundance determined from the CH feature for any of the stellar parameters considered. This test was also conducted for the CN feature and again no noticeable difference was found with varying oxygen abundance. We have assumed that oxygen follows the general α -enhancement trend. That is, $[O/Fe]=0.3$ for objects with metallicities $[Fe/H]\leq-1.0$, and $[O/Fe]=+0.18$ for the higher metallicity stars. ND95 show that there is a number of stars with oxygen deficiencies (values of $[O/Fe]<0.0$) for RGB stars. This indicates that the ON cycle may have occurred in these objects. Although the assumed $[O/Fe]$ abundance does not play a significant role in the abundances determined, it would be beneficial to determine the oxygen abundances for individual stars in future studies.

The stellar parameters derived from the isochrones were used to generate synthetic spectra for ten carbon abundances at each point along an isochrone, for each population. G band indices were determined for each of these synthetic spectra and plotted along with the indices from the observed spectra for each population. This enabled a mean carbon abundance to be obtained for each population, which was then used when another set of synthetic spectra were generated with the nitrogen abundance being the varying parameter. The S3839 index was measured in these synthetic spectra and the results for the synthetic spectra were again plotted with the observed data to obtain a mean nitrogen abundance for each population. This procedure was followed again, but with varying strontium abundance and the strontium indices plotted for the synthetic and observed data.

Interpolation between the synthetic isoindex lines for each element and population enabled a first estimate at the abundances of carbon, nitrogen and strontium for each object. From these abundances the objects with possible enhancements (or in some cases depletions) in carbon, nitrogen and strontium could be identified for further in depth analysis. The synthetic spectra give an initial estimate of the abundances, but should be viewed with caution since there is a 0.4 – 0.6 dex range in $[Fe/H]$ for the member stars of each population but the isoindex lines are for a fixed abundance. Also, some stars have temperatures and gravities that deviate from those used for the isoindex lines. The larger the difference in

[Fe/H], temperature and/or gravity from the isindex value, the larger the uncertainty in the initial estimate.

The C abundance for the synthetic spectra was varied between $[C/Fe]=-0.9$ and $+1.8$. The G band index was measured for each spectrum and plotted with the observed data, shown in the left column of Figure 6. The diamonds represent those stars for which individual abundances were subsequently determined (see §5). The synthetic data for each abundance are plotted as solid lines. A large spread in C abundance can be seen within both the MS stars and the SGB stars and there are two MS stars that have possible enhanced features. The C abundance for the ω Cen stars were calculated by interpolation in luminosity and G band strength to give an initial approximation to the abundance of that element.

The right column of Figure 6 shows the three calibrating globular clusters (NGC 6397, NGC 6752 and 47 Tuc). NGC 6397 and NGC 6752 bracket the metallicity range of the 1st Pop., and their results as normal globular clusters can be compared to those found for ω Cen in order to determine which stars are *abnormal* on the MS of the latter. The error bars in each panel represent errors in measured index and magnitude. They do not include the uncertainty in the inferred abundance induced by an object’s distance in color, magnitude and metallicity from the isochrone used to generate the isindex lines.

The normal globular clusters show no significant spread (1σ) in the CH index, while the first population of ω Cen, on the other hand, shows several objects that are outliers from the bulk of the population and a 2σ spread on the MS and a 4σ spread on the SGB. NGC 6752 can also be compared with the 2nd pop. Again the small spread in the normal GC is in contrast to that seen in ω Cen. The 3rd Pop. can be compared with the results from 47 Tuc, for which the indices have been split according to the CN–CH bimodality for clarity. On close inspection, one sees that the ω Cen results have a similar range in indices to 47 Tuc.

The mean C abundance for the bulk of each population was determined and then used when calculating synthetic spectra with varying nitrogen. Again, the CN index was determined for each synthetic spectrum and plotted against the observed data, shown in the left column of Figure 7. Once more, the error bars in each panel represent errors in measured index and magnitude. The diamonds in this plot indicate those stars that had individual N abundances determined (see §5). As with the plot of the CH indices, the top panel shows the most metal-poor stars, the middle one the intermediate metallicity population, and the bottom panel the most metal-rich stars. Inspection of the top panel shows the synthetic lines for CN are closely spaced on the MS, showing the low sensitivity of the CN feature at these abundances and temperatures. Consequently, finding any objects with high N abundances is difficult, and any spread is comparable to the measurement errors (1σ). Determining N abundances becomes a slightly easier task on the SGB and the presence of several outliers

is clear. The outliers are more pronounced in the 2nd Pop. and there is a large range in apparent N abundance in the 3rd population with 4σ and 9σ spreads on the MS and SGB, respectively. Initial estimates of the N abundance for each ω Cen star were calculated, and all objects with a first pass N abundance, $[\text{N}/\text{Fe}]$, greater than 1.2 dex were included for further study, although this includes a fair number of objects in the metal-poor, MS category that were subsequently shown to have normal N abundances due to the low sensitivity of the feature.

The right column of Figure 7 shows the results for the calibrating globular clusters. Both NGC 6397 and NGC 6752 show little scatter in their indices, as would be expected when the synthetic indices are taken into account. There is very little sensitivity in this feature at these metallicities, temperatures and gravities. ω Cen, as with the G band, shows several stars that have CN indices that are higher than the mean, even with the low sensitivity in this area. The indices for 47 Tuc are again split into the CN–CH bimodality. Two sets of synthetic lines were plotted for these data, with different mean C abundance. We see a larger range within the ω Cen data than for the 47 Tuc indices.

Sr and Ba were analyzed simultaneously, although the Ba index was too weak to obtain meaningful results. The synthetic Sr indices are plotted in the left column of Figure 8 along with the ω Cen data, where the error bars in each panel represent errors in measured index and magnitude. A large spread of the Sr index is apparent in Figure 8, and is mainly due to the low S/N and intermediate resolution of our spectra. The spread in the measured index is comparable to the measurement error in the first two populations. The third population shows a 3σ spread in comparison with the measured errors. Despite this, we are able to identify objects that may have large Sr enhancements, and use these for individual spectrum synthesis analysis. The diamonds represent those objects that had individual Sr abundances calculated, which are discussed in §5.

The normal globular clusters all show no Sr enhancement and any scatter is comparable (of order 1σ) to the measurement errors of the index. 47 Tuc shows several objects that may be considered to have higher Sr abundance ratios, but closer inspection reveals that these objects have higher indices due to low S/N. ω Cen, in all cases, shows larger scatter than the normal globular clusters, with several stars having higher indices being objects of particular interest. Inspection of spectra shows these are not the result of lower S/N.

The choice of isochrones that were used for each of the three populations in the first pass abundance analysis was determined from the mean metallicity and ages of the respective populations. The impact of a different choice of parameters for the three sets of isochrones was evaluated. The first population was assigned an isochrone with $[\text{Fe}/\text{H}]=-1.9$ and age=15 Gyr (as against -1.7 and 13.5 Gyr), the second population an isochrone with $[\text{Fe}/\text{H}]=-1.2$,

age=11 Gyr *cf. –1.4 and 13.0 Gyr) and the third an isochrone with $[Fe/H]=-0.6$ and age=9 Gyr (cf. –0.9 and 12 Gyr). Most stars showed differences in first pass carbon abundances of less than 0.5 dex. Strontium abundances were calculated with differences less than 0.8 dex. Differences in nitrogen values were affected the greatest of the three elements, with differences ranging up to ± 2.0 dex in the most extreme case, and ± 1.0 on average. In practice, the result for the nitrogen abundances was not significant as objects with enhanced N selected for further analysis were determined using the S3839 index rather than the derived N abundance, as described in the following section. The use of a different distance modulus and reddening were also investigated and the differences in derived abundance was found to be less than 0.2 dex for carbon and nitrogen, and less than 0.5 dex for strontium. These differences are all within the error margins placed on the selection of stars with possible enhancements in C, N or Sr.

5. Individual Abundance Analysis

5.1. Abundance Determination of $[C/Fe]$, $[N/Fe]$ and $[Sr/Fe]$

Following the analysis in §4, the subsample of stars with possibly enhanced C, N or Sr abundances were individually analyzed using spectrum synthesis techniques. These objects were chosen according to their first pass abundances. For carbon, if a star’s interpolated abundance was $[C/Fe]>0.3$ it was included. The cutoff for Sr was $[Sr/Fe]>0.8$. The CN index was more complicated due to the weakness of the feature and hence its low sensitivity to C and N. Any interpolated abundance had very large error bars due to the small separation between isoindex lines. Therefore, these objects were chosen based on the S3839 index rather than interpolated abundance and the cutoff imposed was $S3839>-0.05$. All objects in the 3rd Pop. were included for individual analysis.

Stars with $[C/Fe]<-0.75$ from the first pass abundance estimation were also included from the first two populations. However it was found from the comparisons of observed and synthetic spectra for individual stars that in most instances there was not sufficient sensitivity in the data to reliably measure depletions. The low sensitivity of the CN and Sr features on the MS also meant that it was not possible to measure such depletions in N and Sr, respectively, and as such we can not say anything about whether depletions exist amongst these populations.

An age was assigned to each star based on its position on the CMD and metallicity using theoretical isochrones (Yi et al. 2001) as described in Stanford et al. (2006a). It was relatively straightforward to also obtain temperatures and gravities from the isochrones

simultaneously with the ages. A grid of isochrones was used which span the metallicity range $-2.6 < [\text{Fe}/\text{H}] < 0.3$ in 0.05 dex increments. For each metallicity there were 34 isochrones with ages 2–19 Gyrs in 0.5 Gyr steps. Alpha enhancement was taken to be constant ($[\alpha/\text{Fe}]=0.3$) for $[\text{Fe}/\text{H}] \leq -1.0$, and declining linearly for higher $[\text{Fe}/\text{H}]$ until it reached the solar value at $[\text{Fe}/\text{H}]=0$. To assign an age to each star, its metallicity was used to select the nearest isochrone in our grid. The isochrones with this metallicity but with differing ages were then compared to the star’s $(B - V)_0$ and M_V on the CMD to find the one closest. Usually a star’s position did not fall directly on one isochrone and linear interpolation in color or magnitude was performed between the two closest ones to determine its age, along with the temperature and gravity. In almost every case the derived temperature and gravity are not the same as those from the average isochrones used in Figure 3. Comparisons were made with temperatures obtained from color temperature relations in Alonso et al. (1996). These were, on average, smaller by 100K. This value is within the 150K uncertainty in temperature used in the error analysis. Microturbulence was assumed to be 1.0 km s^{-1} .

Each candidate had the abundances of C, N and Sr determined. The C feature (CH) at $\sim 4300\text{\AA}$ was analyzed first. Figure 9 gives examples of a MS star (upper panel) and SGB star (lower panel) with enhancements in carbon. The heavy, solid lines depict the observed spectrum, while the light solid lines show the synthetic spectra. The carbon abundance ratio was modified in the synthetic spectra while all other parameters were held constant. The determined carbon abundance ratio is plotted, along with two others bracketed the value by ± 0.3 dex. A synthetic spectra having $[\text{C}/\text{Fe}]=0.0$ is also shown for comparison.

Given $[\text{C}/\text{Fe}]$, the CN feature at $\sim 3883\text{\AA}$ was used to obtain the N abundances. It proved to be quite difficult to obtain accurate abundances at the resolution of our spectra. There was little sensitivity of the feature at abundances lower than $[\text{N}/\text{Fe}]=1.0$ dex, especially for objects with low $[\text{Fe}/\text{H}]$. Therefore abundances were only recorded when $[\text{N}/\text{Fe}] \geq 1.0$ dex. Figure 10 gives examples of a MS star (top panel) and SGB star (lower panel) with enhancements in nitrogen. The heavy, solid lines indicate the observed spectrum, while the light solid lines show the synthetic spectra. The determined nitrogen abundance ratio is plotted, along with two others bracketing the value by ± 0.3 dex. A synthetic spectrum with $[\text{N}/\text{Fe}]=0.0$ is also shown for comparison.

The Sr abundance was obtained from the Sr II line at 4077\AA line. However, at the S/N of the data it was indistinguishable from the noise at low abundances and results were only recorded when $[\text{Sr}/\text{Fe}] \geq 1.0$ dex. Further, the abundance obtained from this line was only accepted if the (weaker) Sr II line at 4215\AA confirmed the abundance of the first line. The Ba II at 4554\AA line was also examined. However its sensitivity was too low to obtain reliable abundances in most cases. It was able to be used as an extra confirmation of the

Sr abundance, as the Ba abundance is expected to be strongly correlated with that of Sr at these metallicities. Figure 11 gives examples of a MS star (left column) and SGB star (right column) with enhancements in strontium. The heavy, solid lines indicate the observed spectrum, while the light solid lines show the synthetic spectra. The top panels show the Sr II 4077Å line, the middle panels the Sr II 4215 Å one. The strontium abundance ratio determined for these stars is plotted, along with two others bracketing the value by ± 0.3 dex. A synthetic spectrum with $[\text{Sr}/\text{Fe}]=0.0$ is also shown for comparison. The lower panels show the Ba II 4554Å line with the same enhancements in $[\text{Ba}/\text{Fe}]$ as used for $[\text{Sr}/\text{Fe}]$.

5.1.1. Errors

Typical errors were calculated for several objects with different metallicities. The temperature, gravity and metallicity were varied independently. The measured index was also varied by its errors and included in the error calculations. The temperature was varied by 150K, determined by reassigning an isochrone to an individual star based on the error in photometry. The gravity varied by 0.2 dex (determined in a similar way to the uncertainty in temperature), and the metallicity by the individual abundance error for the star being analyzed. The error contributions were added in quadrature. Typical errors were 0.27 dex for the C abundance, 0.37 dex for the N abundance and 0.38 dex for Sr. Note that these errors refer only to the objects that had abundances determined for them.

Abundances were also calculated for a small number of *normal* stars across the three metallicity populations to verify that we would obtain unenhanced abundances for these objects. This was found to be the case, but again the limited sensitivity of the CN and Sr features may not reveal possible enhancements of N and Sr, respectively.

5.1.2. Results

Our abundances are presented in Table 3, which gives the identification number for each star in column 1, and the V magnitude and B–V in columns 2 and 3. The temperature, gravity and metallicity are listed in columns 4–6. In columns 7–10 indices for the G band (CH), S3839 (CN), Sr 4077Å and Ba 4554Å are listed. Abundance ratios of C, N and Sr, relative to iron, are given in columns 11, 12 and 13, respectively, if calculated. To untangle the abundance patterns, each metallicity population was treated separately and abundance information then compared between populations. The positions, photometry, metallicity and ages for these stars are available in the electronic version of Table 2 in Stanford et al.

(2006a).

When performing the spectrum synthesis analysis, comparisons by eye between the Ca II K line in the observed and synthetic spectra were used as a check on the metallicities and temperatures. In a small number of cases there was a large discrepancy between the observed and synthetic, and therefore those stars were not considered further. In total, 32 stars did not have an abundance analysis performed due to unreliable metallicities and/or ages. It is unclear whether the source of the error is driven by the metallicities, related to a 3σ error in the photometry or both. After excluding these stars, this left a total of 392 stars in our sample.

Table 4 gives the number and percentage of normal, C, N and Sr enhancements for each metallicity population. Due to the varying sensitivity of the CH, CN and Sr features, the emphasis of this paper is on objects with enhancements: $[C/Fe] \geq 0.5$ dex, $[N/Fe] \geq 1.0$ dex, and $[Sr/Fe] \geq 1.0$ dex, even though abundance ratios were calculated $\sim 1\sigma$ below these values. These limits were put in place to ensure we had complete numbers of objects within our sample above these values. There are objects with enhancements in carbon and/or nitrogen, and strontium which therefore are counted in both the carbon/nitrogen enhanced and strontium enhanced groups. This means the percentages often sum to more than 100%.

Using a Gaussian distribution with a kernel equal to the error in each abundance, the effect of errors on the number of objects found to be enhanced was investigated. The first distribution was centered at $[C/Fe]=0.0$, with $\sigma_C=0.27$ dex, and produced 5% of the sample as enhanced objects under our criteria of $[C/Fe] \geq 0.5$. This is comparable to the percentage of enhanced objects found on the MS. However, the two metal-poor objects on the MS (9005309 and 7007334, with $[C/Fe]=1.30$ and 1.35, respectively) have $\sim 5\sigma$ C enhancements and are not likely to result from the uncertainties. The number of objects on the SGB that were found to be enhanced is significantly higher than 5%, but may be due to the bias against the bulk of the metal-poor objects in the SGB sample introduced by the blue cutoff at $(B-V)=0.6$ for the 2002 sample.

A similar procedure was employed for the nitrogen and strontium abundances, using $\sigma_N=0.37$ dex and $\sigma_{Sr}=0.38$ dex. Both the N and Sr simulations indicated that it would be unlikely that any objects would be included in the enhanced sample as spurious detections, since less than 1% of the simulated sample had abundances greater than the criteria of $[N/Fe] \geq 1.0$ dex and $[Sr/Fe] \geq 1.0$ dex.

Table 5 lists the abundance patterns found on the main sequence and subgiant branches. One should note that often when we do not find any stars of a particular abundance pattern, it is due to low sensitivity of the relevant observed features. The table only lists numbers of stars

with detectable enhancements of $[C/Fe] \geq 0.5$ dex, $[N/Fe] \geq 1.0$ dex and/or $[Sr/Fe] \geq 1.0$ dex. Due to the selection of the regions on the CMD, meaningful comparisons between the MS and SGB are not possible. The blue color limit for the SGB box is redder than the bulk of the metal-poor population in the cluster. Due to these selection effects there are probably more detections of unusual stars on the SGB than on the MS.

5.2. Abundance Patterns

Figure 12 plots the abundance ratios (relative to iron) of carbon, nitrogen and strontium for each of the three populations, as a function of luminosity. Care must be taken with interpretation of this diagram. The shaded regions in the figure show the areas of limited sensitivity and are plotted below the cutoff values by an amount of $\sigma/2$. Consequently, we do not detect all the enhancements/depletions that are potentially present in our sample. Therefore, only a few conclusions can be drawn from the recorded abundance ratios. Stars have been plotted with different symbols in order to better facilitate the comparisons between different elements and abundances. For the 1st and 2nd populations the open triangles represent those stars that are enriched in carbon ($[C/Fe] \geq 0.5$) and strontium ($[Sr/Fe] \geq 1.0$). Objects that are enhanced in both nitrogen and strontium are shown by solid stars. The one object with enhancements in carbon, nitrogen and strontium, 8001811, is represented by a plus sign inside a circle. All other stars are represented by solid dots with no cross-referencing between panels. Since all stars in the 3rd population have abundance determinations, the symbols are used to show the corresponding object between carbon of any value with enhanced Sr and unenhanced N (as open triangles), or enhanced N and enhanced Sr (as solid stars). Solid triangles represent stars with carbon abundances and nitrogen enhancements that do not have high Sr abundances.

5.2.1. Carbon

Panels a, b and c of Figure 12 show the $[C/Fe]$ abundances for each population. The objects in Fig. 12 with individual abundance determinations are shown as diamonds in the carbon, nitrogen and strontium indices plots (Figures 6, 7 and 8). The reader is reminded that the spectrum synthesis was performed for the entire 3rd Pop. sample, but only for a select group of *enhanced* objects for the 1st and 2nd Pops. Inspection of the C enhanced objects in the 1st Pop. (Fig. 12, panel a) shows there are relatively more objects with elevated abundances on the SGB than on the MS. This same effect is seen to a lesser degree in the 2nd Pop. data in Fig. 12, panel b. If the process that led to the formation of the C-

rich stars was primordial (i.e. they formed from matter already enhanced in C and therefore have uniform abundances throughout) one would expect equal numbers of these objects on the MS and SGB. On the other hand, if these objects had elevated C abundances due to the accretion of material onto their surface layers, as they move off the MS and onto the SGB the convective layer deepens and such enhancements become diminished. Consequently, one would expect not to find as many SGB objects with C enhancements, contradicting the results found here. Instead, the result may be due to the diminished sensitivity of the CH feature on the MS compared with the SGB preventing detection of enhanced C in main sequence objects.

The metal-poor objects on the main sequence with large carbon enhancements are possible counterparts of the CH stars found on the RGB in ω Cen. Two objects on the main sequence, 7007334 ($[C/Fe]=1.35$) and 9005309 ($[C/Fe]=1.30$), seen in Fig. 12 (panel a), show the largest carbon enhancement in our sample, with no other metal-poor main sequence objects showing any enhancement. These objects also show no detectable enhancements of nitrogen or strontium. The study by Bell & Dickens (1974) found that for two of the CH giants in ω Cen (ROA 55 and 70), $[C/H]\sim-0.8$ and $[N/H]\sim0.0$. Adopting $[Fe/H]=-1.9$ for ROA 70 (Gratton 1982), this gives $[C/Fe]\sim1.1$ and $[N/Fe]\sim1.9$. The carbon enhancements are similar to the values found here, although the N enhancement is apparently not, though N sensitivity at this $[Fe/H]$ is low. As for the s-process elements, Gratton (1982) found $[s/Fe]=1.1$ for ROA 70 (where s represents the averaged abundances of the s-process elements), but for our MS stars we do not detect any enhancement of Sr above $[Sr/Fe]=1.0$ dex. A metal-poor SGB star, 8001811, shows enhancements in carbon, nitrogen and strontium, similar to those found for RGB CH stars in ω Cen. This star may also be similar to the “subgiant CH” stars reported by Luck & Bond (1991) in the field, that exhibit carbon and s-process enhancement.

Figure 6 indicates that there are some stars in each of the three populations with possible C depletions. Upon further investigation it was found that in the first population with the lowest metallicities, C abundances were not able to be reliably determined below $[C/Fe]=0.0$ for the majority of candidates. For the second metallicity population, with $-1.5\leq[Fe/H]<-1.1$, $[C/Fe]$ started to lose its sensitivity around -0.2 . C abundances for the most metal-rich population, with $[Fe/H]\geq-1.1$, were able to be determined down to $[C/Fe]\sim-0.7$.

It is significant that we only find one object in the 3rd Pop. with C enhancements greater than 0.0 dex. All objects within the 3rd Pop. went through the individual abundance determination process, although again the CN and Sr features of some objects were not useful for abundance determination. Most of the objects in the 3rd Pop. were C depleted, as can

be seen in the panel c of Fig. 12. Some of these C depleted stars have various large N and/or Sr enhancements. However, it is interesting to note that we find several objects (4/9) with C depletions that do not have corresponding N and/or Sr enhancements. This may be due to the low sensitivity of CN and Sr features.

5.2.2. Nitrogen

Inspection of the middle column of Figure 12 shows the $[N/Fe]$ abundance ratios as functions of luminosity for each of the three populations. The limited sensitivity of the CN feature is indicated by the shaded regions, and for this reason only the extremely N enhanced objects are identified. On the SGB in the metal-poor and metal-intermediate populations it can be seen there is a fraction ($\sim 20\%$) of N enhanced objects, with $[N/Fe]$ up to ~ 2.0 dex. Similarly, the 3rd Pop. contains a significant fraction of objects with N enhancements, of order 50%. These N abundances are ~ 0.5 – 1.0 dex higher than those found for RGB stars in ND95, and up to ~ 0.75 dex higher than in the analysis of RGB stars of Brown & Wallerstein (1993). This large discrepancy between the present work and other studies may be due to differing analysis techniques. Analysis of RGB stars using the method employed here would be useful in resolving this discrepancy.

Nitrogen enhancements are not seen in the 1st Pop. on the MS, although such stars are seen on the SGB at this metallicity and on the MS for the higher abundance groups. Whether this is due to the low sensitivity of the CN feature at the resolution and S/N used here and our subsequent inability to detect the objects with overabundances in N, or is a real effect remains unclear. That said, canonical stellar evolution results do not predict the processing of C to N between the MS and SGB phases of such low mass stars. Only one star on the SGB was found with $[N/Fe] \geq 2.0$. Therefore the fact that no enhancements of $[N/Fe] > 2.0$ were seen for MS stars may be a statistical effect. Higher resolution data are needed to address this question. Piotto et al. (2005), in a study of the double main sequence, found nitrogen enhancements of $[N/Fe] = 1.0$ for the metal-intermediate bMS and $[N/Fe] < 1.0$ for the metal-poor rMS. Therefore it seems likely that our technique, which could only measure enhancements above $[N/Fe] = 1.0$, did not have the required sensitivity to measure any enhancements in N on the main sequence.

5.2.3. Strontium

For Sr there is a abundance trend similar to that found for N across the three populations, as may be seen in Figure 12 (right column). Here one finds a significant number of objects that show Sr enhancement in all three metallicity populations. In particular, we draw attention to the most Sr-rich object, the main sequence star 2015448, which has $[\text{Sr}/\text{Fe}]=1.6$. This object has the added anomalous behavior that while the abundance of Ba usually tracks that of Sr in heavy neutron-capture enhanced objects, we do not detect Ba, and estimate $[\text{Ba}/\text{Fe}]<0.6$. This object is discussed in more detail in Stanford et al. (2006b).

5.2.4. Metal rich Population

The 3rd Pop. differs from the other two populations in that there were essentially no enhancements in C across the MS or SGB. One 3rd Pop. object, 2016543, was identified with mild C enhancement. This object had no N or Sr enhancements.

Figure 13 shows an example of a more typical member of the 3rd Pop, which has depleted carbon ($[\text{C}/\text{Fe}]=-0.4$). This was used to obtain a N abundance from the CN features at 3883Å and 4215Å, yielding $[\text{N}/\text{Fe}]=1.7$ (middle panels). This object also has enhanced Sr and Ba, shown in the lower panels. Another star in our sample, 3001426, has similar stellar parameters and abundances.

6. Discussion

The abundance patterns found here, while somewhat limited, when taken together with the data for the red giants, have the potential to constrain putative sources of enrichment. We begin with a short discussion of possible sources of enrichment and follow with constraints that the present results place on the enrichment processes.

The origin of the abundance enhancements found here are most likely primordial or the result of accretion events. These abundance patterns are unlikely to have been generated within the MS stars themselves as the small convective region does not mix processed materials from the stellar interior to its surface. Comparing these results with those found on the RGB (Smith et al. 1995, ND95) seems to suggest that we are finding similar abundance enhancements in N and the light s-process elements, at least on the SGB. However, most stars studied on the RGB are C depleted, or near solar, and N is enhanced by ~ 1.0 dex (Cohen & Bell 1986; Paltoglou & Norris 1989; Brown & Wallerstein 1993; ND95). In RGB

stars where the C is depleted and N enhanced, the CN and ON cycles have been at work. Whether this was in the stars themselves, in nearby objects whose material was accreted, or occurred in objects from which these stars formed is unclear. However, primordial or accretion of C and/or O is needed to explain the CO-strong stars that exist on the RGB (Persson et al. 1980). While the details of the cluster chemical evolution remain in question, we discuss the various type of objects that might have been responsible for the nucleosynthesis of the various elements that are varying within the system.

6.1. Possible Sources of Enrichment

6.1.1. Low Mass AGB stars

Low mass (1–3 M_{\odot}) AGB stars undergo dredge-up episodes which bring C and s-process elements into the convective region (Gallino et al. 1998). Because of their low mass, these objects do not have hot bottom burning (HBB) episodes which would produce N and reduce C via the CNO cycle. The amount of s-process elements that are produced is dependent on neutron density and the availability of the seed Fe nuclei (Smith 2005). The neutron source is the $^{13}\text{C}(\alpha, n)^{16}\text{O}$ reaction. The s-process is believed to occur in a ^{13}C pocket which is produced at the third dredge-up episode (Gallino et al. 1998; Lattanzio & Lugaro 2005). Specifically, hydrogen downflow from the envelope penetrates the ^{12}C intershell region and at H reignition a ^{13}C enhanced zone is formed. This ^{13}C source releases neutrons giving rise to efficient s-processing that is dependent on the mass fractions of H, ^4He , ^{13}C , ^{14}N and metallicity. For the C enhanced stars where we do not detect any Sr enhancement (s-process), it may be that we simply do not have the sensitivity to detect any enrichment. Alternatively, if there was little or no ^{13}C pocket there was no source of neutrons for the s-process to occur. Thus, depending on the size and efficiency of the ^{13}C pocket, these AGB stars may account for the enhancements of C with and without Sr found in our sample.

6.1.2. Intermediate Mass AGB stars

Intermediate mass (3–8 M_{\odot}) AGB stars are more likely to have HBB, thereby producing a site for the operation of the CN cycle and processing of C into N (Ventura et al. 2002). Production of s-process elements is not expected to be very high in these objects due to the shorter duration of the ^{13}C pocket (Lattanzio et al. 2004). Added to this is lower neutron density from the $^{22}\text{Ne}(\alpha, n)^{25}\text{Mg}$ reaction as the convective region becomes smaller in more massive stars. These stars may account for the objects with N enhancements with little or

no s-process element enhancements.

6.1.3. Massive Stars

Maeder & Meynet (2006) have recently presented models of rotating massive ($\sim 60 M_{\odot}$) stars. These objects produce stellar winds with large excess of He and N, but no C or O excess. Their products are consistent with the abundances seen on the blue main sequence (bMS) (see Piotto et al. 2005), and may be responsible for some of the enhanced objects found here. Recently, abundance patterns of C, N, O, Na and Li obtained from models of fast rotating, massive stars were shown by Decressin et al. (2006) to be similar the chemical anomalies observed in normal globular cluster stars. Whether these two sets of models also synthesize s-process elements is unclear but they may account for objects with enhancements in N.

Smith (2006) discussed the prospect of Wolf-Rayet and OB stars as enrichment sources for globular cluster anomalies. These objects (WN) may produce large amounts of nitrogen, but a top-heavy stellar mass function is required to generate the large amounts of N needed to explain the observations in globular clusters. A similar scenario is needed in the Maeder & Meynet (2006) models.

6.2. Observational Constraints on the Enrichment of ω Cen

Similarities exist between the carbon-rich objects found on the MS and those found on the RGB. Here, two stars out of 195 ($\sim 1\%$) were found to have $[C/Fe] > 1.0$ (these are the metal-poor stars 7007334 and 9005309). There is one possible subgiant CH star, 8001811, which translates to $\sim 0.5\%$ of the total number of SGB stars with CH star properties. These percentages are similar to that found on the RGB for stars brighter than $V \sim 13$ in the Woolley et al. (1966) catalogue, where there are four CH stars (55, 70, 279, 577, see e.g. ND95) out of a possible ~ 600 , equating to 0.7% . This suggests that one might expect to find an approximately one percent incidence of CH stars in any sample at most stages of evolution in the cluster (i.e. excluding blue horizontal branch objects), and indicates that the CH stars are not limited to a particular evolutionary phase.

It is interesting that the C-rich ($[C/Fe] \geq 0.5$) stars occur predominately at low metallicities and we find virtually none in the 3rd Pop. This may result from small number statistics. In the first and second populations we find that 10% of objects have enhanced C. If the same percentage applies to the third population this would equate to only two stars and it is not

outside the realm of possibility that they were simply not found in our search. On the other hand, it may be a result of the material from which these stars formed being low in C to begin with. The source of the carbon enrichment could be low-mass AGB stars or perhaps SNe II. In the latter case, the outer layers escaped while the material close to the iron core did not. Low mass AGB stars also produce s-process elements, depending on initial mass and metallicity. Therefore, they are able to account for the range in s-process enhancement seen in many of the C-rich stars.

Inspection of Figure 12 and Table 4 show there are $\sim 10\%$ of the total sample (excluding the two metal-poor CH stars) with $[C/Fe] \geq 0.5$. This is unusual when compared with the RGB abundances in ω Cen, as previous studies have not found any stars (excluding CH stars) with carbon enhancements at these levels. Carbon abundances of main sequence and subgiant branch stars in other globular clusters also do not show any such enhancements. Carretta et al. (2005) studied carbon, nitrogen and oxygen in dwarfs and subgiant branch stars in NGC 6397, NGC 6752 and 47 Tuc. For dwarfs, carbon abundances were less than $[C/Fe]=0.50$ for NGC 6397, $[C/Fe]=0.2$ for NGC 6752 and $[C/Fe]=-0.1$ for 47 Tuc. The subgiants showed abundance levels of $[C/Fe] \leq 0.15$ for NGC 6397, and $[C/Fe] \leq -0.10$ for NGC 6752 and 47 Tuc.

These C enhanced objects on the MSTO of ω Cen may be the evolutionary precursors to the CO-strong objects on the RGB (Persson et al. 1980). Of the stars that are investigated in Persson et al. (1980), 28 come from the unbiased sample of Cannon & Stobie (1973). The CO-strong stars represent 8 out of these 28 stars, or $\sim 30\%$ of RGB objects. If the 10% of C-rich ($[C/Fe] \geq 0.5$) stars found on the MSTO are the evolutionary precursors, one would expect that more of these objects should have been found. However, our choice of the C-rich cutoff (at $[C/Fe]=0.5$) is arbitrary and it is not known what the link is between CO-strong status and carbon abundance on the MSTO. If the C-rich cutoff was lower we would have found a higher percentage of objects that are C-rich on the MSTO. It would be useful in future investigations to determine carbon abundances for the whole sample to confirm the connection between the C-enhanced objects at the MSTO and the CO-strong objects on the RGB.

The carbon abundances found here in the 3rd Pop. are low when compared with those determined for dwarfs by Carretta et al. (2005) in NGC 6397, NGC 6752 and 47 Tuc. The lowest abundances found for NGC 6752 and 47 Tuc were $[C/Fe]=-0.2$ and $[C/Fe]=-0.13$, respectively. The origin of these depletions for the most metal-rich group is not well understood. Pancino (2003) did not investigate carbon abundances for the most metal-rich RGB sample in ω Cen, and of the few metal-rich RGB stars studied by ND95 carbon abundances were found to be $[C/Fe] \sim -0.3$. If evolutionary mixing on ascent of the RGB occurred, one

would expect even lower carbon abundances than those found on the MS, but for the two metal-rich RGB stars studied by ND95 this was not found to be the case. Estimates of the level of carbon depletions for the 1st and 2nd Pops. would be of great interest to be able to compare them not only with those found in the 3rd Pop., but also with those on the RGB. Piotto et al. (2005) found $[C/Fe]=0.0$ for both the metal-poor and metal-intermediate main sequences (rMS and bMS, respectively) using composite spectra of stars belonging to both populations.

The nitrogen enhancements seen at the MSTO across all three populations are quite substantial with $[N/Fe]$ as large as 2.2. These abundances are slightly larger than those seen in other clusters (Carretta et al. 2005). The nitrogen enhancements in NGC 6752 reach $[N/Fe]=1.7$ for dwarfs and $[N/Fe]=1.3$ for subgiants. The maximum N enhancements for 47 Tuc are lower and only reach $[N/Fe]=1.1$ for the subgiants, while our third population shows enhancements greater than $[N/Fe]=1.1$ for 37.5% of the group. Piotto et al. (2005) investigated the two distinct main sequences in ω Cen and found abundances of C, N and Ba using composite spectra of a number of stars in each sequence. They found $[N/Fe]\sim 1.0$ for the blue main sequence (bMS), which is equivalent in metallicity to the 2nd Pop. discussed here. This is lower by a factor of 3–10 for the abundances of N found here. This may be due to a systematic offset in the abundances found here compared with those found by Piotto et al. (2005). On the ω Cen RGB, ND95 also found N abundances to be less than those found here by ~ 0.7 dex.

While Sr abundances have not been extensively investigated on the RGB, lines of other light s-process elements such as Y and Zr have been analyzed (ND95 Smith et al. 1995, 2000). In general, it was found that the abundance of the s-process elements relative to iron increased as a function of metallicity. There are no correlations of s-process elemental abundances with other light elements where variations are seen, such as C, N, O, Na and Al (ND95). Qualitatively, this is similar to what is found here. The incidence of Sr enhancement relative to iron increases as a function of metallicity (see Table 4). This fits in with the idea that low to intermediate mass AGB stars contributed to the gas from which the later generations of stars formed. A comparison between the Sr abundances found for RGB and MS stars will be discussed further in a forthcoming paper (Stanford et al. 2007, in preparation).

It is not clear if intermediate mass AGB stars are responsible since s-processing is not very efficient in these objects. To account for the N and Sr enhanced stars favorable conditions of N and s-process element production in intermediate mass AGB stars are needed. Alternatively, the enriched objects may be accounted for by several different sources. For instance, massive rotating stars may account for the N overabundances while low-mass AGB may account for the s-process enrichment. This latter scenario is supported by the fact that

no strong correlation is seen between nitrogen and strontium (s-process) abundances.

Other globular clusters, that do not show metallicity (i.e. iron) spreads, show variations in the abundances of light elements to varying degrees, as described in §1. Several clusters show CN–CH bimodality not only on the RGB but also on the MS (Cannon et al 1998; Briley et al 2004; Suntzeff & Smith 1991; Gratton et al 2001a; Cohen 1999; Briley & Cohen 2001; Ramírez & Cohen 2002; Cohen, Briley & Stetson 2002; Briley, Cohen & Stetson 2004; Da Costa et al. 2004). In this respect, the spread in C and N on the MSTO of ω Cen is not unique and these results demonstrate the variations are a product of environment since field stars do not show similar patterns. Variations in other light elements such as Na, O, Mg and Al are also found on the MS in some clusters (Gratton et al 2001b). These elements have yet to be studied on the MS level in ω Cen to determine if the same effect is seen in this cluster. The theoretical yields of AGB stars at present fail to explain the abundance patterns seen in the light elements in globular clusters (see e.g. Fenner et al. 2004). That is, there is more to the enrichment scenario in other clusters that is yet to be explained and this complication may also be the case for ω Cen.

6.2.1. Constraints on the Role of Binarity

If the enhancements are due to past accretion events as part of binary systems, the fraction of objects with overabundances indicates ω Cen should have a large binary fraction, of order $\sim 20\%$. In a radial velocity study of red giants in ω Cen spanning over a decade, Mayor et al. (1996) estimated the global binary frequency is 3–4%. Further, they reported that most of the giants with known chemical peculiarities, such as Ba, CH and S stars, have constant velocities, suggesting that they are not members of binary systems. However, there is the possibility that these objects may have been former binaries that were disrupted by close encounters with nearby stars. The same argument can be applied to the MS stars, where the fraction of C, N and Sr enhanced stars exceeds the observed binary frequency for giants in the cluster.

7. Conclusion

A low resolution spectroscopic abundance analysis of a sample of 392 ω Cen members revealed objects enhanced in carbon, nitrogen and/or strontium. These enhanced objects were analyzed in detail and abundances ratios of carbon, nitrogen and strontium relative to iron determined. The abundances revealed patterns that can possibly be explained by

low and intermediate mass AGB and/or rotating massive star nucleosynthesis. The enhancements are either primordial or from accretion events, rather than evolutionary. Higher resolution, and higher S/N data are needed to further constrain the possible sources of these abundances anomalies. From such data, abundances of a large number of elements such as the light elements (O, Na, Mg, Al), other light and heavy s-process elements, and iron peak elements, will be essential in obtaining another piece of the ω Cen puzzle.

We thank the Director and staff of the Anglo-Australian Observatory for the use of their facilities.

REFERENCES

- Alonso, A., Arribas, S., Martinez-Roger, C. 1996, *A&A*, 313, 873
- Anderson, J., 2002, in van Leeuwen, F., Hughes, J. D., & Piotto, G., eds., *ASP Conf. Ser.* Vol. 265, *A Unique Window into Astrophysics.* (Astron. Soc. Pac.: San Francisco), 87
- Beckers, J. M., Bridges, C. A., & Gilliam, L. B. 1976, *A high resolution spectral atlas of the solar irradiance from 380 to 700 nanometers.* (Hanscom AFB, MS: Sacramento Peak Obs.)
- Bedin, L. R., Piotto, G., Anderson, J., Cassisi, S., King, I. R., Momany, Y., & Carraro, G. 2004, *ApJ*, 605, L125
- Beers, T. C. & Christlieb, N. 2005, *ARA&A*, 43, 531
- Beers, T. C., Rossi, S., Norris, J. E., Ryan, S. G., & Shefler, T. 1999, *AJ*, 117, 981
- Bekki, K., & Norris, J. E. 2006, *ApJ*, 637, L109
- Bell, R. A., & Dickens, R. J. 1974, *MNRAS*, 166, 89
- Bessell, M. S., & Norris, J. 1976, *ApJ*, 208, 369
- Briley, M. M., & Cohen, J. G. 2001, *AJ*, 122, 242
- Briley, M. M., Cohen, J. G., & Stetson, P. B. 2004, *AJ*, 127, 1579
- Briley, M. M., Harbeck, D., Smith, G. H., & Grebel, E. K. 2004, *AJ*, 127, 1588
- Brown, J. A., & Wallerstein, G. 1993, *AJ*, 106, 133

- Butler, D., Dickens, R. J., & Epps, E. 1978, *ApJ*, 225, 148
- Cameron, A. G. W. 1982, *Ap&SS*, 82 123
- Cannon, R. D., Croke, B. F. W., Bell, R. A., Hesser, J. E., & Stathakis, R. A. 1998, *MNRAS*, 298, 601
- Cannon, R. D., & Stobie, R. S. 1973, *MNRAS*, 162, 207
- Carretta, E., Gratton, R. G., Bragaglia, A., Bonifacio, P., & Pasquini, L. 2004, *A&A*, 416, 925
- Carretta, E., Gratton, R. G., Lucatello, S., Bragaglia, A., & Bonifacio, P. 2005, *A&A*, 433, 597
- Cohen, J. G. 1999, *AJ*, 117, 2434
- Cohen, J. G., & Bell, R. A. 1986, *ApJ*, 305, 698
- Cohen, J. G., Briley, M. M., & Stetson, P. B. 2002, *AJ*, 123, 2525
- Cottrell, P. & Norris, J. 1978, *ApJ*, 221, 893
- Cunha, K., Smith, V. V., Suntzeff, N. B., Norris, J. E., Da Costa, G. S., & Plez, B. 2002, *AJ*, 124, 379
- Da Costa, G. S., Cannon, R. D., Croke, B., & Norris, J. E. 2004, *Mem. Soc. Astron. Italiana*, 75, 370
- Da Costa, G. S. & Demarque, P. 1982, *ApJ*, 259, 193
- Da Costa, G. S., Stanford, L. M., Norris, J. E., Cannon, R. D. 2005, in *IAU Symposium No. 228, From Lithium to Uranium: Elemental Tracers of Early Cosmic Evolution.*, Hill, V., Francois, P., & Primas, F., eds., 369, Cambridge: Cambridge University Press
- Decressin, T., Meynet, G., Charbonnel, C., Prantzos, N., & Ekström, S. 2006, *astro-ph/0611379*
- Dickens, R. J., & Bell, R. A. 1976, *ApJ*, 207, 506
- Dinescu, D. I., van Altena, W. F., Girard, T. M., & López, C. E. 1999, *AJ*, 117, 277
- Fenner, Y., Campbell, S. W., Karakas, A. I., Lattanzio, J. C., & Gibson, B. C. 2004, *MNRAS*, 353, 789

- Francois, P., Spite, M., & Spite, F. 1988, *A&A*, 191, 267
- Freeman, K. C., & Rodgers, A. W. 1975, *ApJ*, 201, L71
- Gallino, R., Arlandini, C., Busson, M., Lugaro, M., Travaglio, C., Straniero, O., Chieffi, A., & Limongi, M. 1998, *ApJ*, 497, 388
- Gratton, R. G. 1982, *A&A*, 115, 336
- Gratton, R. G., Bonifacio, P., Bragaglia, A., Carretta, E., Castellani, V., Centurion, M., Chieffi, A., Claudi, R., Clementini, G., D'Antona, F., Desidera, S., Francois, P., Grunahl, F., Lucatello, S., Molaro, P., Pasquini, L., Sneden, C., Spite, F., & Straniero, O. 2001, *A&A*, 369, 87
- Gratton, R. G., Sneden, C., Carretta, E., & Bragaglia, A. 2001, *A&A*, 354, 169
- Harris, W. E., 1996, *AJ*, 112, 1478
- Hilker, M., & Richtler, T. 2000, *A&A*, 362, 895
- Langer, G. E., Kraft, R. P., Carbon, D. F., Friel, E., & Oke, J. B. *PASP*, 1986, 98
- Lattanzio, J., Karakas, A., Campbell, S., Elliot, L., & Chieffi, A. 2004, *Mem. Soc. Astron. Italiana*, 75, 322
- Lattanzio, J. C., & Lugaro, M. A. 2005, *NuPhA*, 758, L477
- Lee, Y.-W., Joo, J.-M., Sohn, Y.-J., Rey, S.-C., Lee, H.-C., Walker, A. R. 1999, *Nature*, 402, 55
- Lewis et al., 2002, *MNRAS*, 333, 279
- Lloyd Evans, T. 1977, *MNRAS*, 181, 591
- Lub, J., 2002, in *ASP Conf. Ser. Vol. 265, A Unique Window into Astrophysics*. van Leeuwen, F., Hughes, J. D., & Piotto, G., eds., (Astron. Soc. Pac.: San Francisco), 95
- Luck, R. E., & Bond, H. E. 1991, *ApJS*, 77, 515
- Maeder, A., & Meynet, G. 2006, *A&A*, 448, L37
- Mayor, M., Duguennoy, A., Udry, S., Anderson, J., & Nordstrom, B. 1996, *ASP Conf. Ser. Vol. 90, The Origins, Evolution, and Destinies of Binary Stars in Clusters*, in Milone, G., & Mermillod, J.-C., eds., (Astron. Soc. Pac.: San Francisco), 190

- Norris, J. E. 2004, ApJ, 612, L25
- Norris, J., & Bessell, M. S. 1975, ApJ, 201, L75
- Norris, J. E., Cottrell, P. L., Freeman, K. C., Da Costa, G. S. 1981, ApJ, 244, 205
- Norris, J. E., & Da Costa, G. S. 1995, ApJ, 447, 680
- Norris, J. E., & Da Costa, G. S. 1995, ApJ, 441, L81, ND95
- Norris, J. E., Freeman, K. C., & Mighell, K. J. 1996, ApJ, 462, 241
- Norris, J. E., Ryan, S. G., & Beers, T. C. 1997, ApJ, 488, 350
- Paltoglou, G., & Norris, J. E. 1989, ApJ, 336, 185
- Pancino, E. 2003, Ph.D. Thesis, Univ. Bologna
- Pancino, E., Ferraro, F. R., Bellazzini, M., Piotto, G., & Zoccali, M. 2000, ApJ, 534, 83
- Pancino, E., Pasquini, L., Hill, V., Ferraro, F. R., Bellazzini, M. 2002, ApJ, 568, L101
- Persson, S. E., Frogel, J. A., Cohen, J. G., Aaronson, M., & Matthews, K. 1980, ApJ, 235, 452
- Piotto, G., Villanova, S., Bedin, L. R., Gratton, R., Cassisi, S., Momany, Y., Recio-Blanco, A., Lucatello, S., Anderson, J., King, I. R., Peitrinferni, A. & Carraro, G. 2005, ApJ, 621, 777
- Ramírez, S. V. & Cohen J. G. 20002, AJ, 123, 3277
- Rey, S.-C., Lee, Y.-W., Ree, C. H., Joo, M.-J., & Sohn, Y.-J. 2004, AJ, 127, 958
- Smith, G. H. 2006, PASP, 118, 1225
- Smith, V. V. 2005, in ASP Conf. Ser. Vol. 336, Cosmic Abundances as Records of Stellar Evolution and Nucleosynthesis in honor of David L. Lambert. Barnes, T. G. & Bash, F. N., eds., (Astron. Soc. Pac.: San Francisco), 165
- Smith, V. V., Cunha, K., & Lambert, D. 1995, AJ, 110, 2827
- Smith, V. V., Suntzeff, N., Cunha, K., Gallino, R., Busso, M., Lambert, D., & Straniero, O. 2000, AJ, 119, 1239
- Sollima, A., Ferraro, F. R., Pancino, E. & Bellazzini, M. 2005, MNRAS, 357, 265

- Stanford, L. M., Da Costa, G. S., Norris, J. E., & Cannon, R. D. 2006a, *ApJ*, 647, 1075
- Stanford, L. M., Da Costa, G. S., Norris, J. E., & Cannon, R. D. 2006b, *ApJ*, 653, L117
- Suntzeff, N. B., & Kraft, R., P. 1996, *AJ*, 111, 1913
- Suntzeff, N. B., & Smith, V. V. 1991, *ApJ*, 381, 160
- Ventura, P., D’Antona, F., & Mazzitelli, I. 2002, *A&A*, 393, 215
- Woolley, R. v. d. R., et al. 1996, *R. Obs. Ann.*, No 2
- Yi, S., Demarque, P., Kim, Y.-C., Lee, Y.-W., Ree, C.-H., Lejeune, T., & Barnes, S. 2001, *ApJ*, 136, 417

Table 1: Line Index Wavelength Bands (\AA)

Line (1)	Line Band (2)	Blue Sideband (3)	Red Sideband (4)
CH – G band	4292.5-4317.5	4247.0-4267.0	4357.0-4372.0
Sr II 4077	4074.7-4080.7	4048.0-4060.0	4085.0-4092.0
Sr II 4215	4212.0-4218.0	4201.0-4211.0	4245.0-4257.0
Ba II 4554	4551.0-4557.0	4505.0-4512.0	4573.0-4579.0

Table 2: Solar abundances and gf values used for s-process elements.

Line (1)	$\log(N/N_{tot})_{\odot}$ (2)	gf value (3)
Sr II 4077	–9.10	1.0460
Sr II 4215	–9.10	0.7161
Ba II 4554	–9.85	1.7050

Table 3. Stellar parameters, Indices and Abundances for ω Cen sample. The full version of this table appears in the electronic version

ID	V mag	B–V	Teff	logg	[Fe/H]	G Band	S3839	Sr 4077 \AA	Ba 4554 \AA	[C/Fe]	[N/Fe]	[Sr/Fe]
(1)	(2)	(3)	(4)	(5)	(6)	(7)	(8)	(9)	(10)	(11)	(12)	(13)
1000812	17.470	0.610	5874	3.8	–1.64	1.42	–0.06	0.19	0.09
1002064	18.290	0.570	6066	4.3	–1.41	2.42	–0.06	0.28	0.09
1002884	17.490	0.600	5901	3.8	–1.76	1.51	–0.11	0.11	0.19
1004374	17.500	0.620	5883	3.8	–1.72	2.71	–0.14	0.18	0.20	0.50	0.00	0.00
1005088	17.390	0.730	5443	3.6	–1.58	5.79	–0.06	0.18	0.29
1005996	17.320	0.720	5572	3.7	–1.49	4.95	–0.10	0.37	0.24
1006065	17.510	0.650	5761	3.8	–1.62	2.48	–0.01	0.11	0.04
1006286	17.380	0.710	5564	3.7	–1.49	4.64	–0.04	0.29	0.28
1006625	17.540	0.610	5869	3.8	–1.78	2.07	–0.11	0.06	0.19
1006759	18.120	0.510	6282	4.2	–1.71	0.73	–0.10	0.07	0.22
1006812	17.430	0.640	5772	3.8	–1.49	2.71	–0.07	0.07	0.25
1006962	17.870	0.670	5672	3.9	–1.59	4.43	–0.11	0.41	0.29	0.40	0.50	1.40
1007266	18.430	0.530	6179	4.3	–1.50	0.74	–0.13	–0.09	0.08
1007362	17.450	0.680	5681	3.7	–1.65	4.29	–0.10	0.29	0.12	0.50	0.00	0.00
1007414	17.840	0.630	5869	3.9	–1.44	2.89	–0.13	0.25	0.27

Table 4. Enhancement of C, N and Sr statistics.

Sample	Total #		Normal		[C/Fe] \geq 0.5		[N/Fe] \geq 1.0		[Sr/Fe] \geq 1.0	
	MS	SGB	MS	SGB	MS	SGB	MS	SGB	MS	SGB
Full Sample	195	197	88.2%	65.0%	4.1%	16.8%	6.2%	16.2%	5.1%	14.2%
1st Population ¹	116	118	97.4%	75.4%	1.7%	14.4%	0.0%	8.5%	0.9%	9.3%
2nd Population ¹	61	73	80.3%	49.3%	8.2%	21.9%	9.8%	26.0%	8.2%	19.2%
3rd Population ¹	18	6	55.6%	50.0%	5.6%	0.0%	33.3%	50.0%	22.2%	50.0%

¹1st Population: [Fe/H] $<$ -1.5; 2nd Population: $-1.5\leq$ [Fe/H] $<$ -1.1; 3rd Population: [Fe/H] \geq -1.1

Table 5. Abundance Patterns found on the Main Sequence of ω Cen.

Abundance Pattern ¹	1st Pop. ²		2nd Pop. ²		3rd Pop. ²	
	MS	SGB	MS	SGB	MS	SGB
C only enh.	2	13	3	10	1	0
C + N enh.	0	0	0	0	0	0
C + Sr enh.	0	3	2	6	0	0
C + N + Sr enh.	0	1	0	0	0	0
Total C enh.	2	17	5	16	1	0
N only enh.	0	5	4	13	3	0
N + C enh.	0	0	0	0	0	0
N + Sr enh.	0	4	2	6	3	3
N + C + Sr enh.	0	1	0	0	0	0
Total N enh.	0	10	6	18	6	3
Sr only enh.	1	3	1	2	3	0
Sr + C enh.	0	3	2	6	0	0
Sr + N enh.	0	4	2	6	3	3
Sr + C + N enh.	0	1	0	0	0	0
Total Sr enh.	1	11	5	14	6	3
C depl. only	0	0	0	0	4	0
C depl. + N enh.	0	0	0	0	3	0
C depl. + Sr enh.	0	0	0	0	1	0
C depl. + N + Sr enh.	0	0	0	0	1	2
Total C dep.	0	0	0	0	9	2

¹Carbon enhanced: [C/Fe] \geq 0.5; Nitrogen enhanced: [N/Fe] \geq 1.0; Strontium enhanced: [Sr/Fe] \geq 1.0; Carbon depleted: [C/Fe] \leq -0.2

²1st Pop.: [Fe/H] $<$ -1.5; 2nd Pop.: $-1.5\leq$ [Fe/H] $<$ -1.1; 3rd Pop.: [Fe/H] \geq -1.1

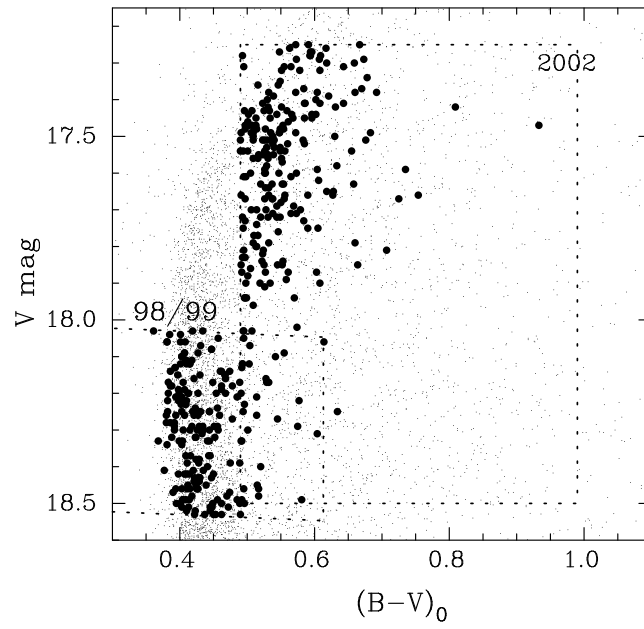


Fig. 1.— Color-magnitude diagram for stars near the MSTO and subgiant branch of ω Cen. Large circles denote stars which are radial velocity members from two samples selected within the regions outlined.

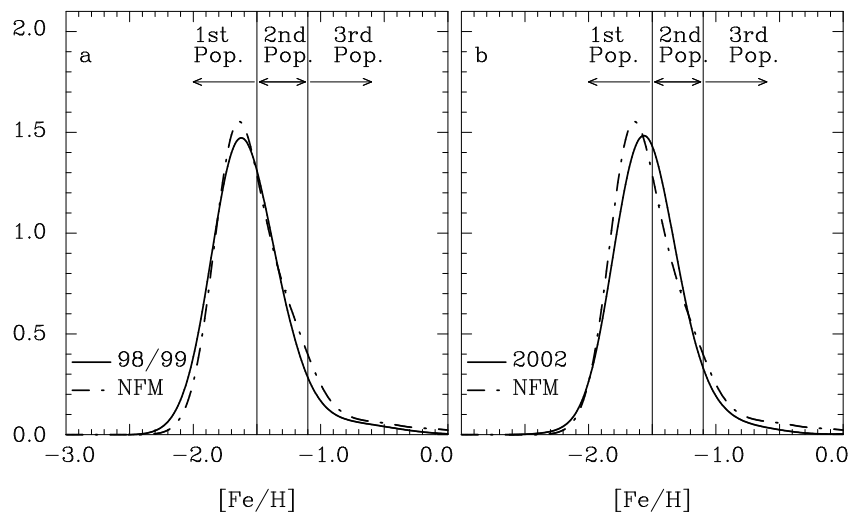


Fig. 2.— Generalized histograms of the metallicity distribution for the 98/99 (panel a) and 2002 (panel b) samples (gaussian kernel of $\sigma=0.15$ – 0.20 , based on the individual errors for each metallicity). For comparison, the Norris, Freeman & Mighell (1996) red giant branch distribution is also plotted ($\sigma=0.14$). Indicated on each histogram is the division into three populations with the first having $[Fe/H] < -1.5$, the second $-1.5 \leq [Fe/H] < -1.1$, and the third $[Fe/H] \geq -1.1$.

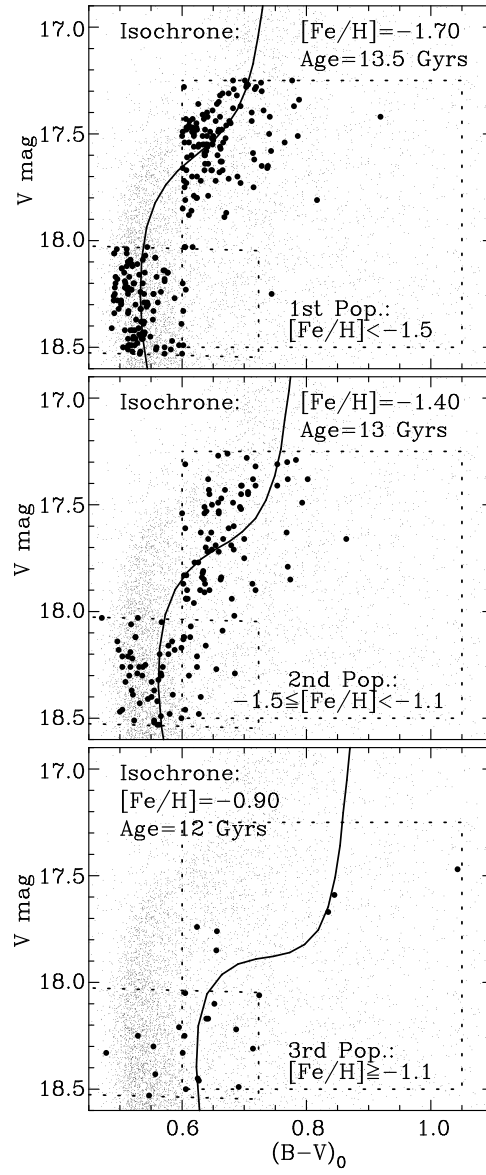


Fig. 3.— Color-magnitude diagrams of the three populations of ω Cen defined by their metallicities. Isochrones with metallicities and ages representing the means of each population are also plotted.

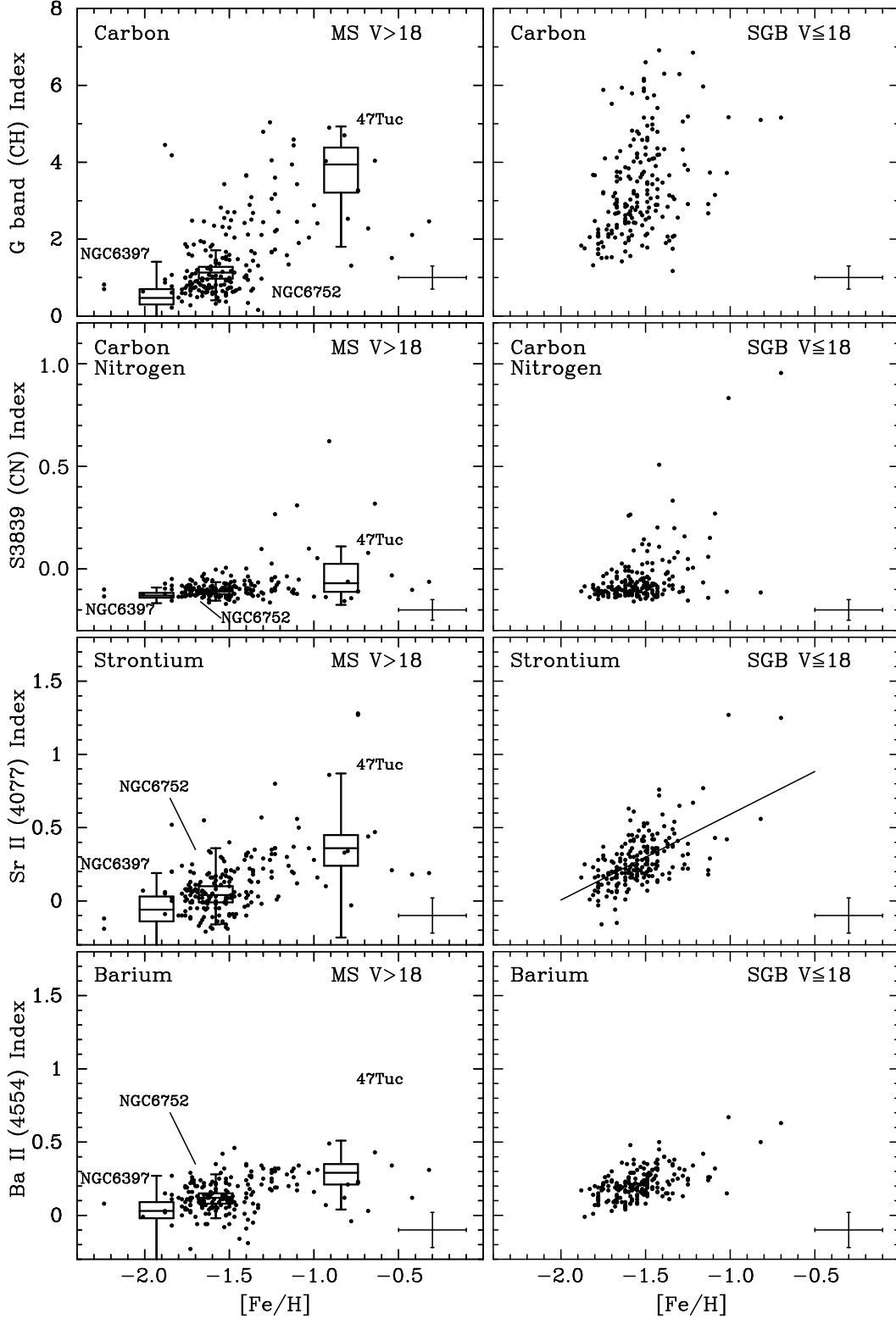


Fig. 4.— Indices for the G band (CH), CN at $\sim 3883\text{\AA}$, Sr II 4077\AA and Ba II 4554\AA , plotted against metallicity for the main sequence ($V > 18$) and subgiant branch stars ($V \leq 18$). The boxed regions on the MS plot represent indices calculated for three other globular clusters — NGC 6397 ($[\text{Fe}/\text{H}] = -1.96$), NGC 6752 ($[\text{Fe}/\text{H}] = -1.56$) and 47 Tuc ($[\text{Fe}/\text{H}] = -0.76$).

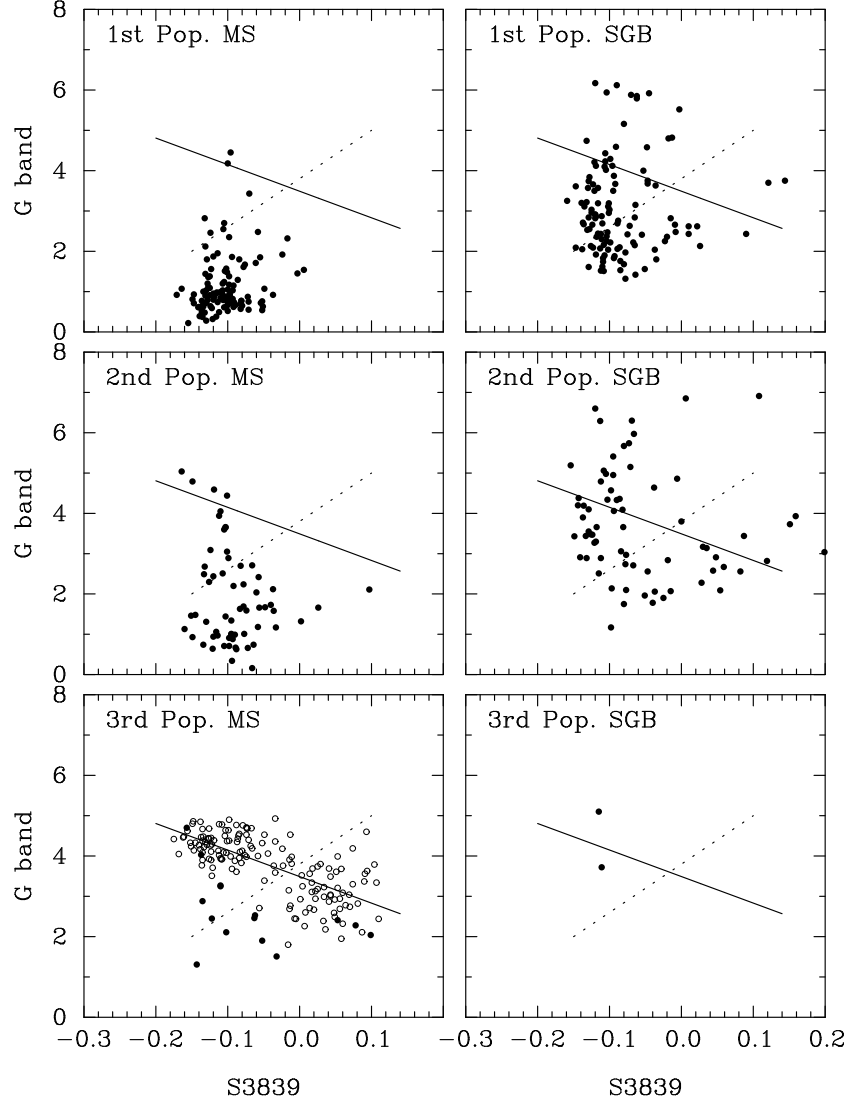


Fig. 5.— CN vs CH indices for ω Cen (solid dots) and 47 Tuc (open circles). The 47 Tuc data, plotted only in the metal-rich, MS panel, are split according to the CN/CH bimodality with the division shown by the dotted line defined in the bottom left panel, and reproduced in the other panels. The solid line is a fit to the CN, CH anticorrelation and plotted in each panel as a reference. The ω Cen data are divided according to metallicity and position on the CMD (MS or SGB).

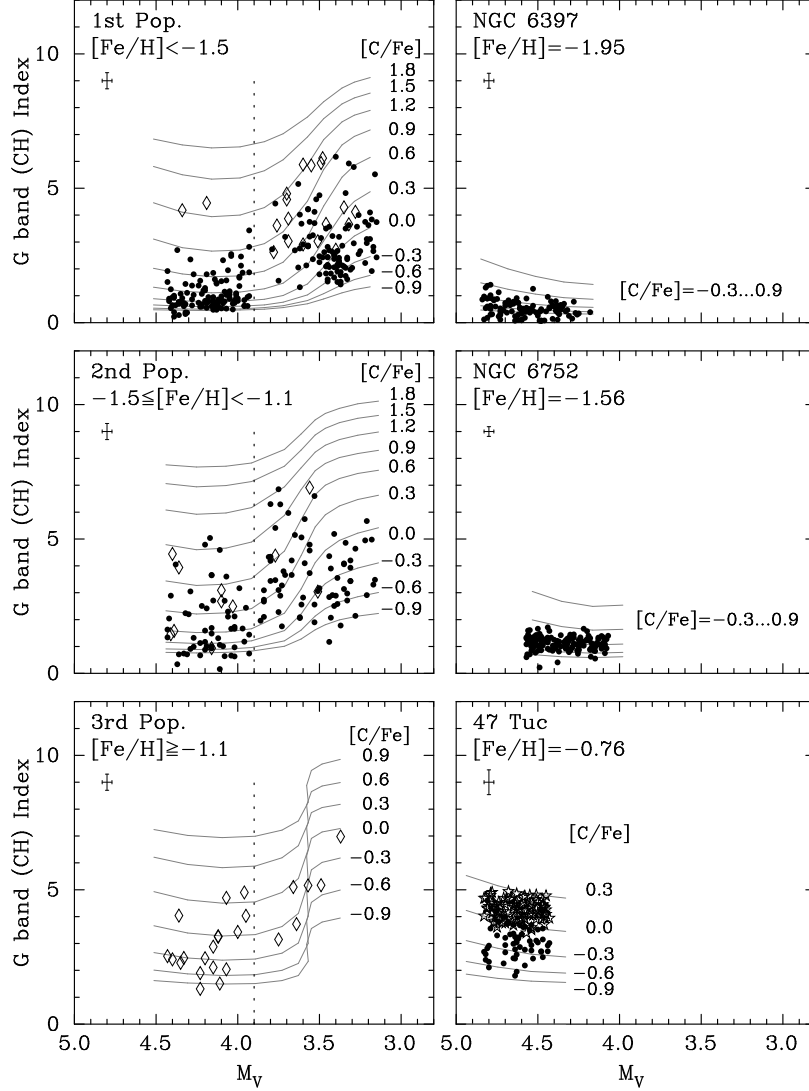


Fig. 6.— G band indices plotted against absolute magnitude (M_V) for each of the three populations of ω Cen in the left panels, and calibrating globular clusters in the right panels. The diamonds represent those stars for which individual abundances were determined, while filled circles represent all other objects. Lines of common abundance are also plotted for the synthetic spectra. The vertical dashed line represents the cutoff between main sequence and turnoff stars. See text for details.

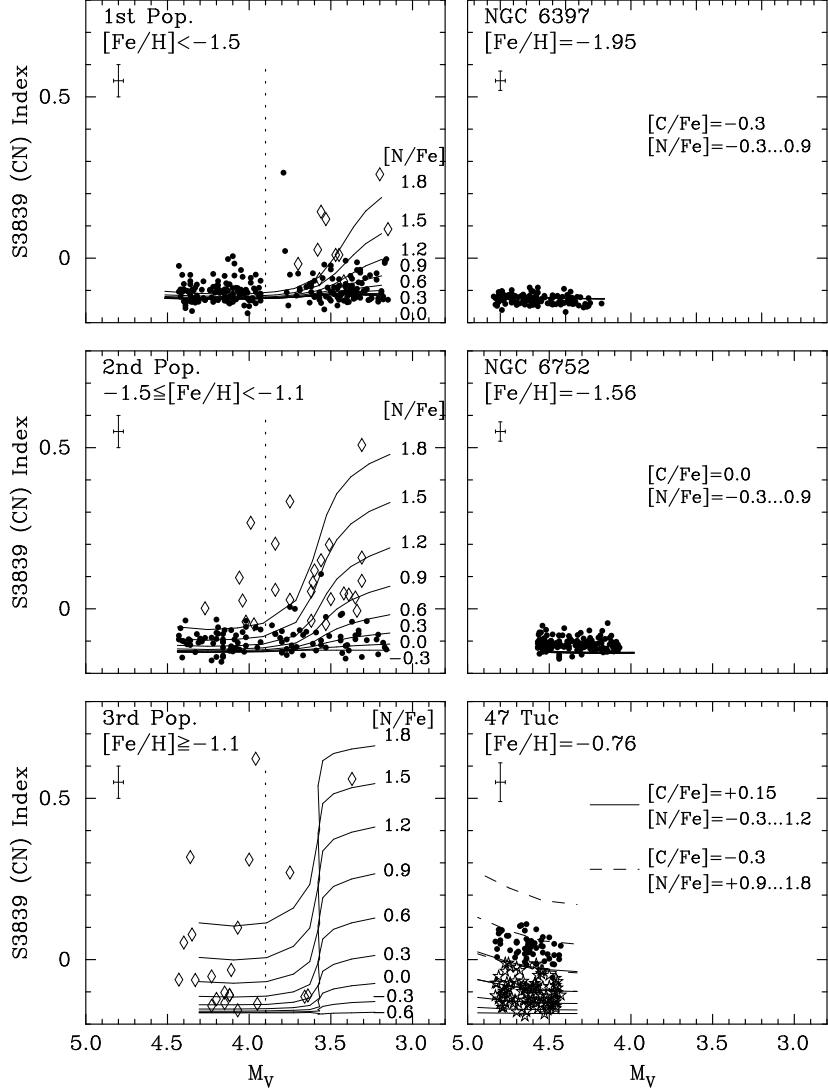


Fig. 7.— CN indices plotted against absolute magnitude (M_V) for each of the three populations in the left hand panels and the calibrating globular clusters in the right. The diamonds represent those stars for which individual abundances were determined, while filled circles represent all other objects. Lines of common abundance are also plotted for the synthetic spectra. The vertical dashed line represents the cutoff between main sequence and turnoff stars. See text for details.

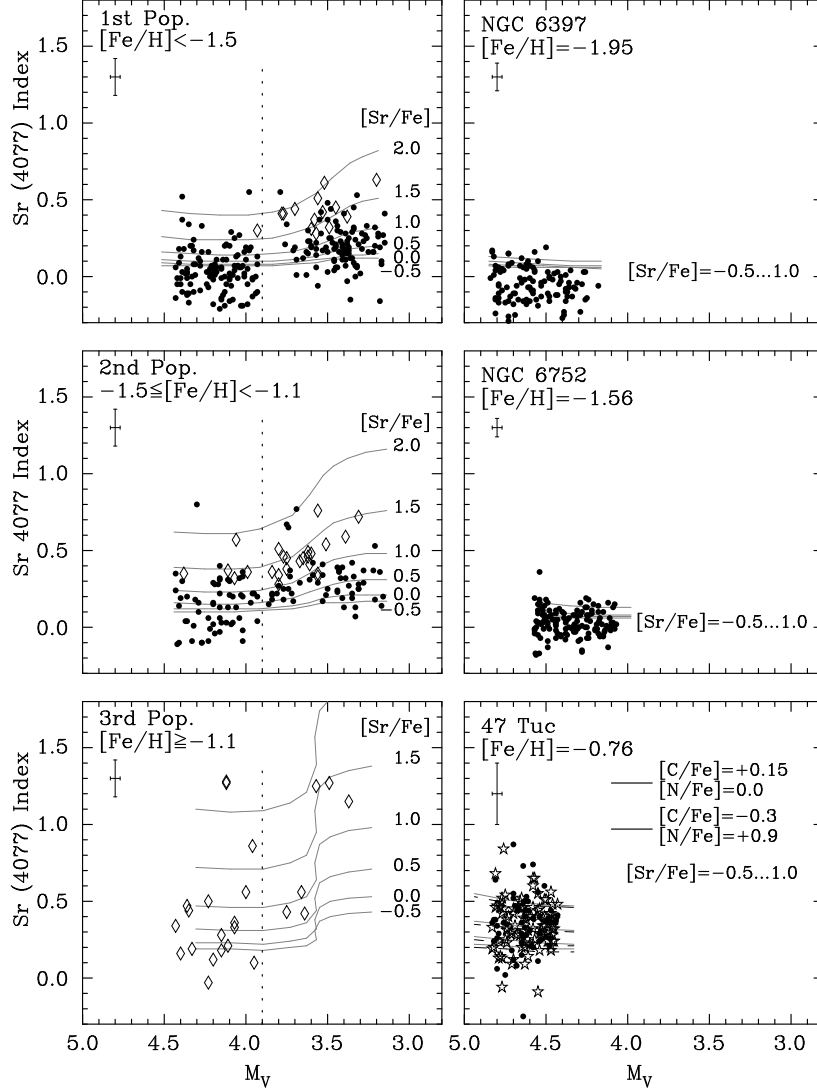


Fig. 8.— Sr II 4077Å, indices plotted against absolute magnitude (M_V) for each of the three populations in the left hand panels and the calibrating globular clusters in the right. The diamonds represent those stars for which individual abundances were determined, while filled circles represent all other objects. Lines of common abundance are also plotted for the synthetic spectra. The vertical dashed line represents the cutoff between main sequence and turnoff stars. See text for details.

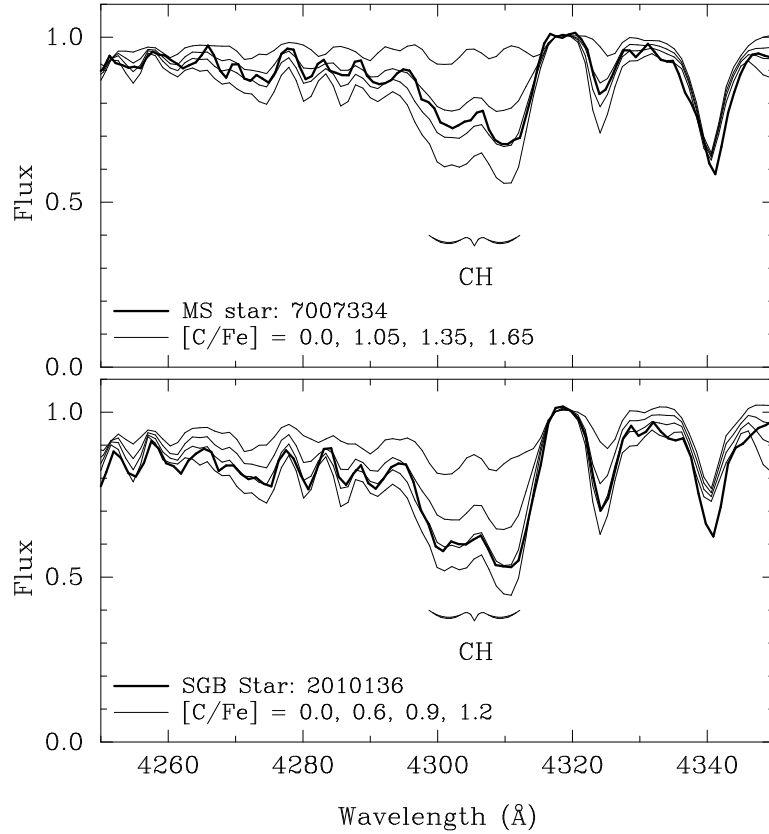


Fig. 9.— Examples of observed and synthetic spectra for two objects with enhanced carbon abundances. The bold line represents the observed spectrum in each case. The top panel shows an example of a MS star, 7007334, with $[C/Fe]=1.35$, while the lower panel shows a SGB star, 2010136, with $[C/Fe]=0.9$. Synthetic spectra with four carbon abundances are shown for each object, including $[C/Fe]=0.0$ for completeness.

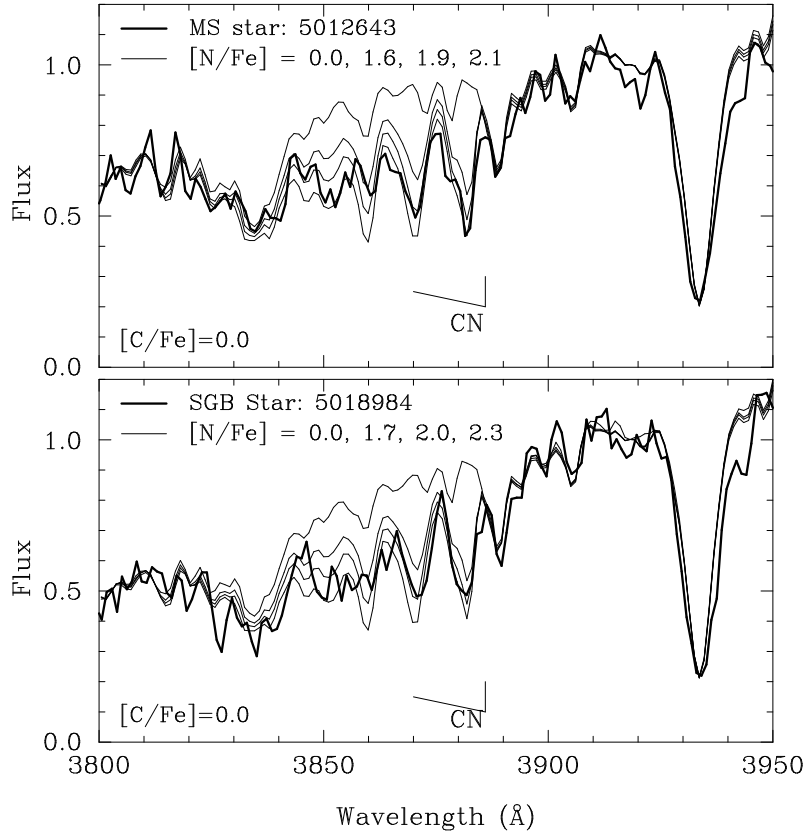


Fig. 10.— Example observed and synthetic spectra of two objects with enhanced nitrogen abundances. The top panel shows the spectrum of a MS star in bold, 5012643, and synthetic spectra as light lines for a range of nitrogen abundances including $[N/Fe]=0.0$. The bottom panel shows a SGB star, 5018984, with $[N/Fe]=2.0$ dex. For both stars, $[C/Fe]=0.0$.

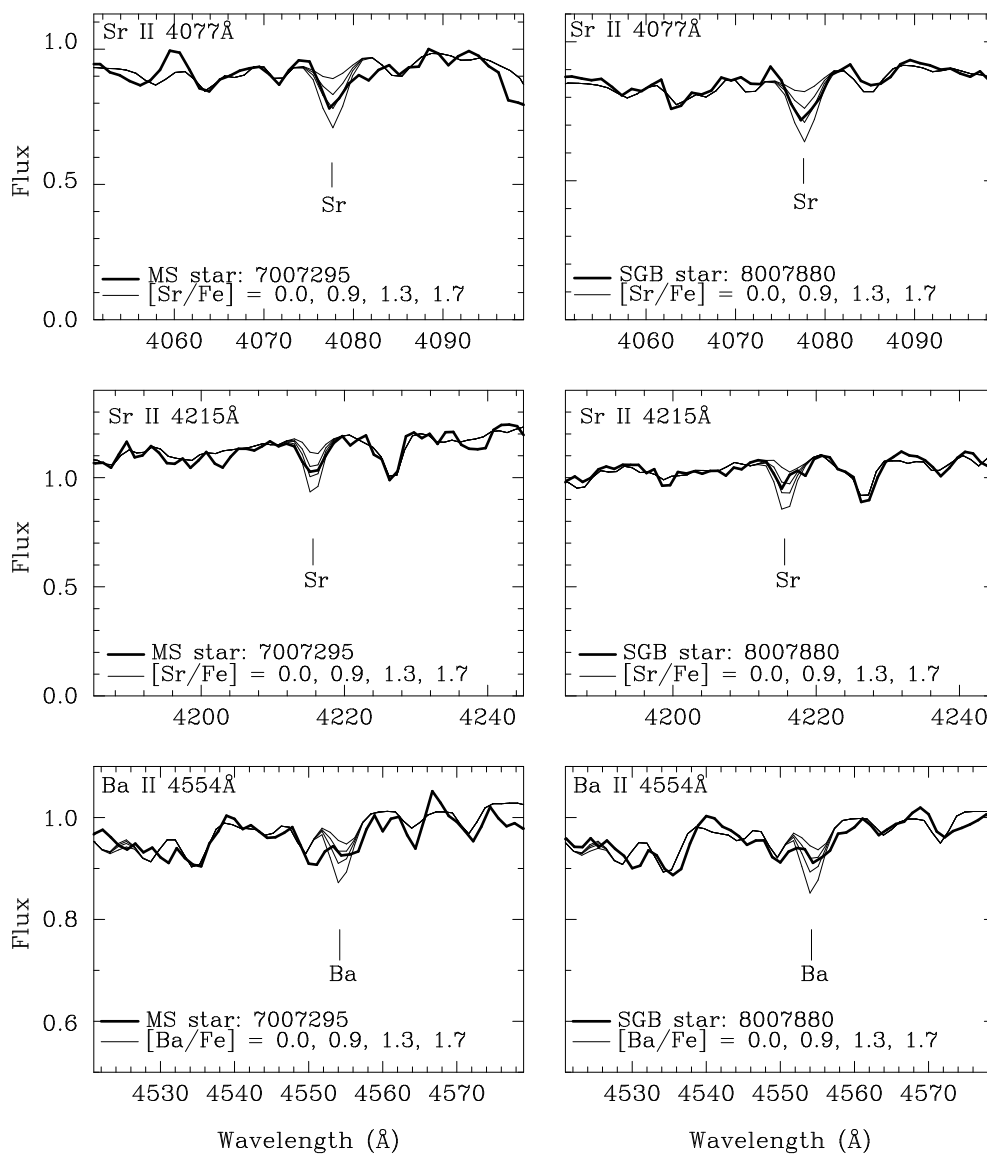


Fig. 11.— Observed and synthetic spectra showing a MS object, 7007295, on the left. The right panel shows a SGB star, 8007880, with enhanced s-process elements. The top panel in each shows the Sr II 4077Å line, the middle shows Sr II 4215Å and the bottom shows Ba II 4554Å.

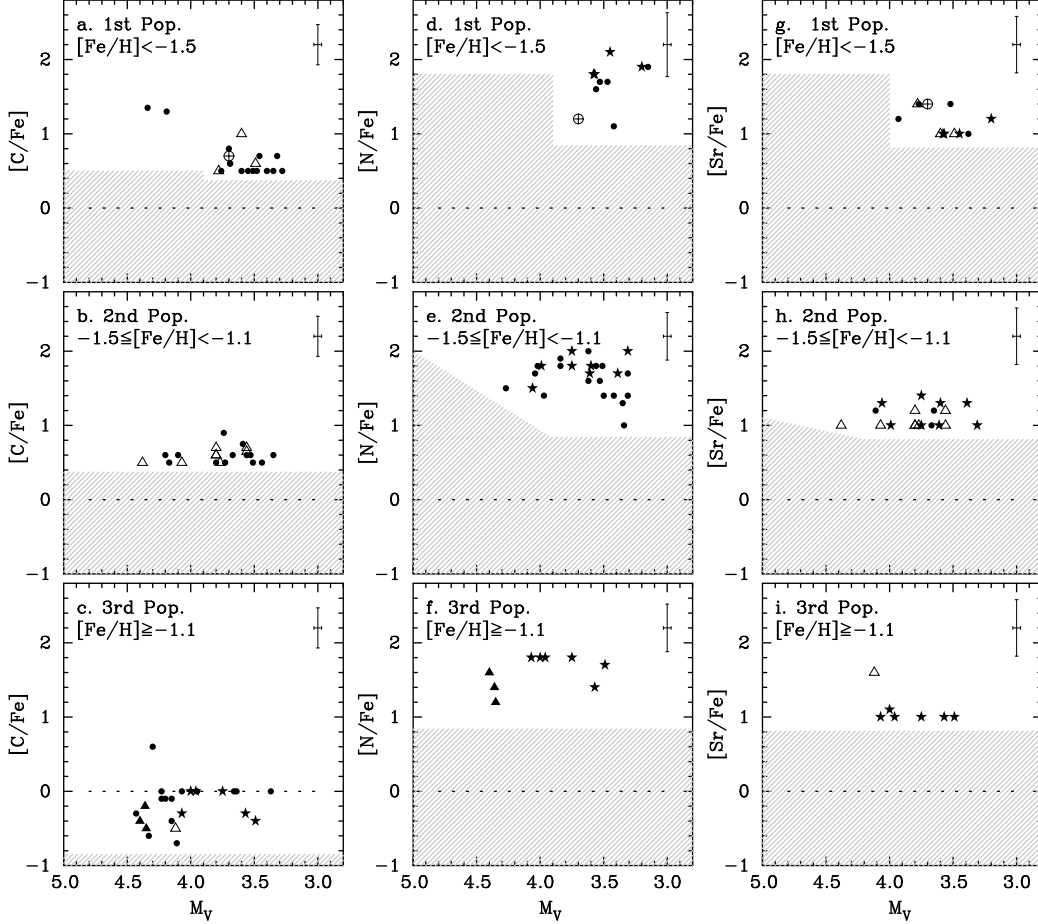


Fig. 12.— Abundance ratios (relative to Fe) of C, N and Sr for the three metallicity populations as a function of magnitude. The shaded regions indicate areas of low sensitivity where the abundances are not able to be determined reliably, and as such care should be taken in interpretation of the abundance patterns. The dotted horizontal line represents solar abundance ratios. For main sequence stars $V > 18$ ($M_V > 4.04$) and turnoff stars $V \leq 18$ ($M_V \leq 4.04$). Also, one should note the limited sensitivity of the CN and Sr features, particularly at low metallicities, which makes it difficult to recognize all objects of interest. Finally, the biased color selection of the SGB sample that excludes many metal-poor stars should not be overlooked. In particular, comparisons between the MS and SGB groups should not be made. See text for more details for definitions of the symbols.

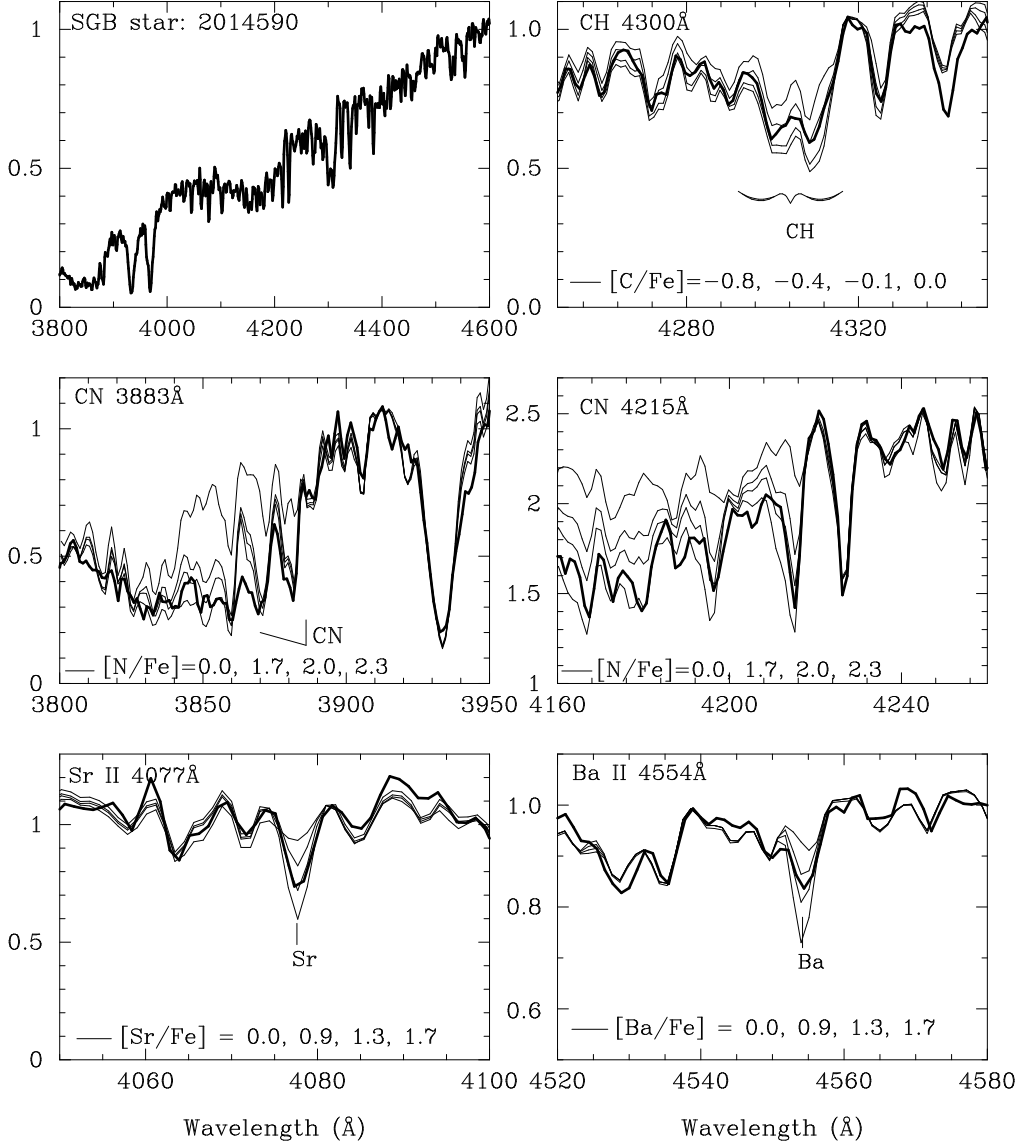


Fig. 13.— Observed and synthetic spectra of star 2014590 from the most metal-rich population, with $[Fe/H] = -1.0$ dex. The top left panel shows the spectrum of this object in the range 3800–4600 Å. The top right panel shows the observed spectrum (bold line) with synthetic spectra (light lines) in the region of the G band. The middle two panels show the CN features at ~ 3883 Å (left panel) and ~ 4216 Å (right panel). The bottom left panel shows the Sr II 4077 Å line and the bottom right panel shows Ba II 4554 Å.